Frontiers of Magnetic Force Microscopy

O. Kazakova[1], R. Puttock[1,2], C. Barton[1], H. Corte-León[1], M. Jaafar[3], V. Neu[4], and A. Asenjo[3]

[1]*National Physical Laboratory, Hampton Road, TW11 0LW, Teddington, United Kingdom*

[2]*Departent of Physics, Royal Holloway University of London, Egham, TW20 0EX, United Kingdom*

[3]*CSIC, Campus Cantoblanco, 28049 Madrid, Spain*

[4]*Leibniz Institute for Solid State and Materials Research, Dresden, 01069, Germany*

Cite as: J. Appl. Phys. 125, 060901 (2019); https://doi.org/10.1063/1.5050712
Submitted: 02 August 2018. Accepted: 12 January 2019. Published Online: 08 February 2019.
https://aip.scitation.org/doi/10.1063/1.5050712

ABSTRACT

Since it was first demonstrated in 1987, magnetic force microscopy (MFM) has become a truly wide-spread and commonly used characterization technique that has been applied to a variety of research and industrial applications. Some of the main advantages of the method includes its high spatial resolution (<50 nm), ability to work in variable temperature and applied magnetic fields, versatility and simplicity in operation; all without almost any need for sample preparation. However, for most commercial systems, the technique has historically provided only qualitative information, and the number of available modes was typically limited thus not reflecting the experimental demands. Additionally, the range of samples under study were largely restricted to 'classic' ferromagnetic samples (typically, thin films or patterned nanostructures).

Throughout this Perspective article the recent progress and development of MFM is described, followed by a summary of the current state-of-the-art techniques and objects for study. Finally, the future of this fascinating field is discussed in the context of emerging instrumental and material developments. Aspects including quantitative MFM, the accurate interpretation of the MFM images, new instrumentation, probe-engineering alternatives, and applications of MFM to new (often interdisciplinary) areas of the material science, physics and biology will be discussed.

We first describe the physical principals of MFM, specifically paying attention to common artefacts frequently occurring in MFM measurements; then we present a comprehensive review of the recent developments in the MFM modes, instrumentation and the main application areas; finally, the importance of the technique is speculated upon for emerging or anticipated to emerge fields including skyrmions, 2D-materials and topological insulators.

1. INTRODUCTION

First demonstrated in 1987[1,2], magnetic force microscopy (MFM) is a well-established and widely used technique. Over the last three decades, the method has been extensively used in a vast number of applications where the knowledge of the local distribution of the magnetic properties of thin film materials and their nanostructures is of paramount importance. This functional technique relies on quantifying the long-range

magnetostatic force between the magnetic sample and a magnetically coated probe positioned at a constant height over the specimen surface. In its simplest form, the typical MFM procedure involves two linear scans. Firstly, the topography of the surface is obtained by using tapping mode atomic force microscopy (AFM) (i.e. exploiting van der Waals interactions between the probe and sample). During the second scan, the probe is lifted away from the sample [i.e. van der Waals interactions are negligible and the probe experiences only long-range magnetic (and electrostatic) interactions] and the initial topography profile is repeated at the constant lift scan height (Fig. 1a).

The knowledge and expertise accumulated in the initial period of MFM development established a fundamental base for the modern commercial MFM systems. However until recently, unlike other functional scanning probe microscopy (SPM) techniques, commercial MFM systems have not demonstrated a variety of modes and were used primarily on their own. At the same time, the use of MFM was somewhat limited to 'classic' ferromagnetic (FM) samples, although they were represented in a variety of forms. Recently, the rise of novel materials, often combining magnetic and other functional properties or demonstrating complex forms of magnetism, such as multiferroics, topological insulators, magnetic semiconductors, etc., has stimulated a burst in the development of advanced MFM modes.

A number of methods have been developed to image magnetic structures with different sensitivities and on many lateral scales. These methods can be roughly divided into beam- and scanning probe-based techniques. The former involves a broad spectrum of physical principals of operation (i.e. polarized light, x-rays, and electrons) and includes both well-established and novel techniques such as magneto-optical microscopy based on Kerr and Faraday effects[3,4], Lorentz force microscopy[5], scanning electron microscopy (SEM) with polarization analysis[6,7], and photoemission electron microscopy[8,9], specifically including x-ray magnetic linear and circular dichroism microscopy[10].

The latter group comprises a variety of magnetically sensitive SPM-based techniques. One of the recent exciting examples includes integration of nitrogen vacancy (NV) defect centers with high-Q diamond mechanical oscillators, allowing realization of a quantum qubit system with the advantages of highly coherent electron spin and narrow optical transitions; accompanied by nanometer scale resolution[11,12]. Another example is magnetic resonance force microscopy that succeeded in detecting single electrons and small nuclear spin ensembles[13,14]. Successful examples of mounting a magnetic sensor on a scanning probe include Hall probe microscopy[15] and superconducting quantum interference device (SQUID) microscopy[16–18]. All these methods have both advantages and drawbacks, as well as a different degree of application in research and industry. These techniques are, however, beyond the scope of this Perspectives article, which will entirely focus at on MFM.

MFM has been most widely used for local characterization of magnetic nanostructures and imaging the magnetic field distribution at the surface of magnetic materials[1,2,19]. Despite decades of advances in magnetic imaging[20], obtaining direct, uncoupled and quantitative information with high spatial resolution remains an outstanding challenge.

Among all methods for the observation of magnetic domain structures, MFM is the most widely used, due to its high spatial resolution (~ 10 nm)[21], sensitivity (~10 pN)[22], relative simplicity in sample preparation, capability to apply *in situ* magnetic fields to study magnetization processes[23] and can operate in different environments[24].

The MFM technique has been proven as an excellent characterization tool in both fundamental research and industrial applications. For comprehensive MFM reviews performed in the early days of MFM, see [21,25,26].

The aim of this Perspective article is to analyze recent progress in development of MFM, present the current state-of-the-art, and outline the future and perspective of this fascinating field. Such emerging aspects as probe-engineering alternatives, new instrumentation, quantitative measurements, the correct interpretation of the resulting MFM images, the loss of energy analysis and applications of MFM to new emerging areas of the material science, physics and biology, etc., are subjects of ongoing research that will be discussed in this work.

The article is organized as following: Chapter 2 describes the physical principals of MFM, and common artefacts in MFM measurement; the review (Chapter 3) describes the recent developments in instrumentation and the main application areas; finally, the perspective (Chapter 4) presents the emerging trends in the field of MFM.

2. PRINCIPLES AND ARTEFACTS IN MFM

The long-range force interactions (i.e. force gradients) between the magnetic probe and the magnetic sample in MFM are recorded and correlated in the second pass from the shift in frequency ($\Delta\omega$), amplitude (ΔA), or phase ($\Delta\phi$) from the initial driven parameters (i.e. ω_0, A_0 and ϕ_0, respectively) of the oscillating cantilever. However, it is not possible to directly quantify these tip-sample interactions without prior knowledge of the probe properties and behavior. In the absence of any tip-sample interactions, the oscillating probe can be approximated as a point-mass spring, thus can be defined by a classic non-linear, second order differential equation, i.e. from Newton's second law of motion[27]. From the possible recorded data channels above, $\Delta\phi$ of the cantilever is the most common representation of magnetic contrast in the second-pass of MFM, hence it is useful to describe the relationship between the phase in free space (ϕ_f) and the excitation frequency (ω) without any externally acting forces as[28,29]

$$\phi_f(\omega) = \tan^{-1}\left(\frac{m\omega\omega_0}{Q(k-m\omega^2)}\right) \quad [1]$$

$$k = m\omega^2, \quad [2]$$

where m, ω_0, Q and k are the point mass, resonant angular frequency, quality factor and the spring constant of the cantilever, respectively. When the probe is oscillated at $\omega = \omega_0$, equation 1 dictates $\phi_f(\omega)$ is equal to $\frac{\pi}{2}$ rad. If we introduce tip-sample interactions (F_{ts}), this subtly changes the oscillation and subsequently the instrument response. Assuming small displacements (z) with respect to the rest position (z_0) of the cantilever, the force can be described as follows after a Taylor expansion[30],

$$F_{ts} \approx \left.\frac{dF_{ts}(z)}{dz}\right|_{z=z_0} z(t), \quad [3]$$

thus the equation of motion is adapted to encompass the sum of the force derivatives acting on the cantilever,

$$F_0\cos(\omega t) = mz''(t) + \frac{m\omega_0}{Q}z' + \left[\left(k - \frac{dF_{ts}}{dz}(z)\right)z(t)\right]. \quad [4]$$

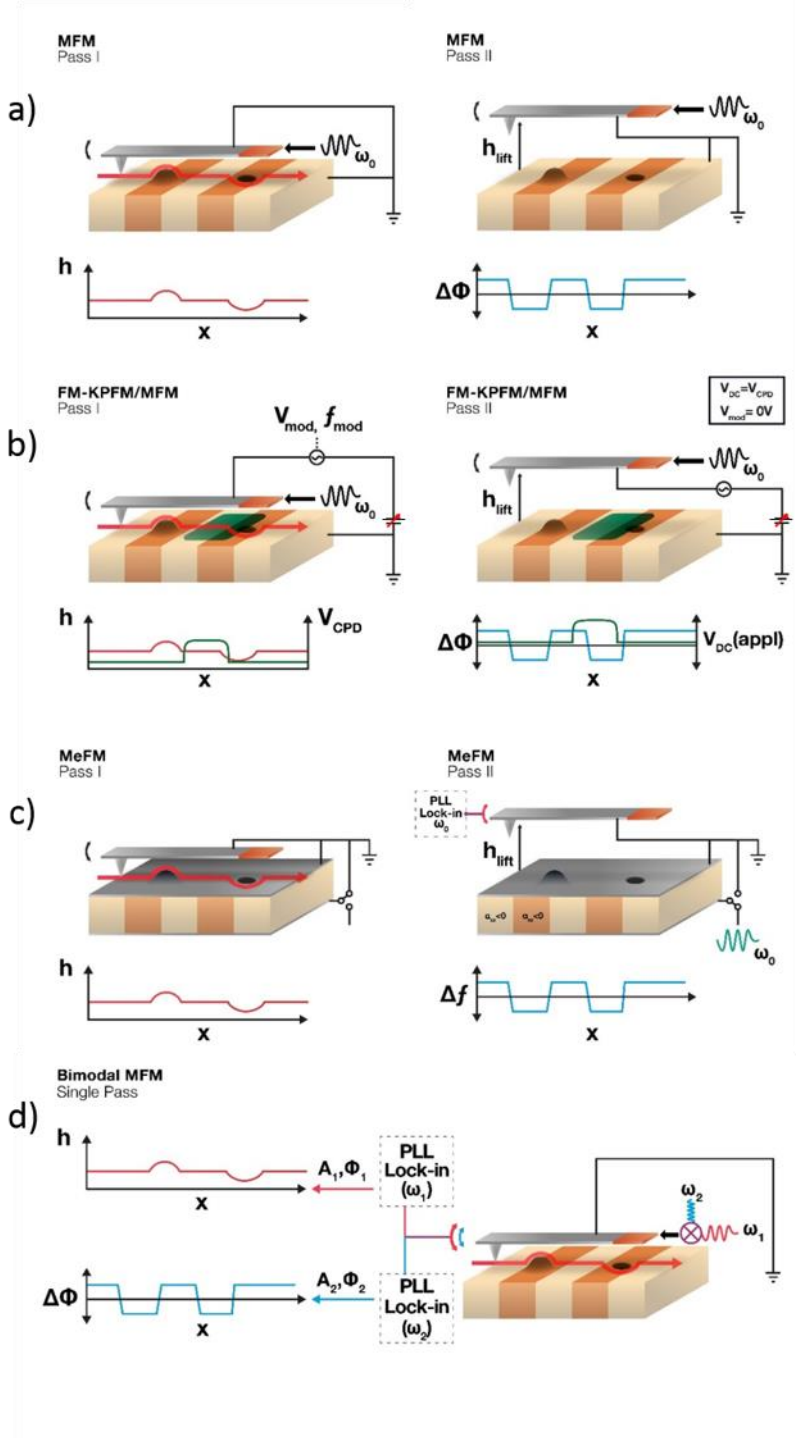

Figure 1: Schematics for different MFM modes. **(a) Standard two-pass MFM**: In the first pass (left) the probe raster scans the surface, mapping the topography of the sample by "tapping" along the surface at its resonant frequency (ω_0); in the second pass (right) the probe lifts a set distance away from the sample (h_{lift}) and maps the long-range interactions, via the phase change of the oscillating cantilever, at a constant probe-sample separation. **(b) Frequency-modulated Kelvin probe force microscopy-MFM**: In addition to acquiring the sample topography in the first-pass (left), the technique is sensitive to the probe-sample contact potential difference (CPD) by monitoring the magnitude of the sidebands of the probe's resonant peak induced from a modulated AC-voltage (V_{mod}, f_{mod}) applied to the probe; the effects of the CPD are nullified in the second-pass (right) by applying a DC-voltage of magnitude such that the sidebands are effectively reduced to zero (i.e. $V_{DC} = V_{CPD}$). **(c) Dynamic magnetoelectric force microscopy:** The first pass (left) is the same as in (a); in the second-pass (right) the probe is not mechanically oscillated, instead a combined AC/DC bias is applied to the sample base-electrode and the sample potential is electrically modulated at the mechanical resonance of the cantilever (ω_0). The resulting AC

magnetic field from the sample (from the linear magnetoelectric effect) induces resonant motion of the magnetic probe. **(d) Bimodal MFM:** A single-pass technique where the probe is excited at (two of its resonant frequencies (ω_1 and ω_2), each of these frequencies are sensitive to specific sample properties (e.g. short- and long-range probe sample interactions.

"σ" is utilized here is because a number of possible forces can be acting between the probe and the sample simultaneously, including van der Waal, magnetostatic and electrostatic interactions. In order to isolate solely the magnetic contrast, methods must be utilized to mitigate the parasitic signals (discussed in greater detail in the review section). In equation 4, F_0 describes the amplitude of the driving force, and $\frac{m\omega_0}{Q}$ represents the damping factor. Equation 1 in the presence of σ becomes

$$\phi(\omega) = \tan^{-1}\left(\frac{m\omega\omega_0}{Q(k+\sigma-m\omega^2)}\right), \quad [5]$$

which, providing the probe is oscillated at ω_0 and $\sigma << k$, equation 2 can be substituted into equation 5 and gives us the phase as a function of σ:

$$\phi(\omega_0) = \tan^{-1}\left(\frac{k}{Q\sigma}\right). \quad [6]$$

Combining equations 1 and 6 finally produces the approximate relation between the $\Delta\phi$ and σ, [29]

$$\Delta\phi(\omega_0) = \frac{\pi}{2} - \tan^{-1}\left(\frac{k}{Q\sigma}\right) \approx \frac{Q}{k}\sigma. \quad [7]$$

An understanding of how the cantilever resonant frequency shifts from ω_0 is also desirable, as frequency-modulated modes in MFM and other scanning probe techniques are becoming more common. The $\Delta\omega$ can be detected by classical lock-in techniques and signal can be utilized for greater parameter control, e.g. more controlled tip-sample distance control (e.g. from capacitive coupling)[31]. Here we'll succinctly describe the relation of $\Delta\omega$ to σ. From equation 4 it is possible to define the effective spring constant of the cantilever (k_{eff}) as[30,32,33],

$$k_{\text{eff}} = k - \sigma(z)|_{z=z_0}, \quad [8]$$

where a positive (attractive) or negative (repulsive) force gradient effectively leads to a softer or harder cantilever, respectively[27,30]. This modification hence causes a shift in ω_0 to ω'_0 in equation 2, thus

$$\omega'_0 = \left(\frac{k-\sigma}{m}\right)^{\frac{1}{2}} = \omega_0\left(1-\frac{\sigma}{k}\right)^{\frac{1}{2}} \quad [9]$$

Assuming once again that $\sigma << k$, a Taylor expansion can be performed on equation 9 and $\Delta\omega$ is finally given by

$$\Delta\omega \approx -\frac{\omega_0\sigma}{2k}. \quad [10]$$

Relating the calculated force gradients to quantitative descriptions of a sample's magnetic parameters is a further field of research, requiring an estimation of the MFM probe's magnetic parameters from which to decouple from the acquired MFM dataset. A further discussion of how this is achieved is outlined in section 3b.

Despite the advantages highlighted throughout this article, MFM is not without its limitations and errors. Just like other SPM techniques, MFM is susceptible to artefacts, which can perturb the measured image and, without careful handling, can lead to incorrect interpretation of the results. Many common SPM-based artefacts and methods for reducing their effects are discussed elsewhere[34]. Table I summarizes MFM-specific artefacts and solutions to minimize their effects on recorded images. A number of these will be specifically discussed throughout the present work.

Arguably the most important factor for accurately representing stray magnetic fields emanating from the measurand is careful consideration of the probe and its own magnetic and physical properties relative to the sample. The resolution and sensitivity of MFM probes are primarily governed by the tip's shape and magnetic properties. However, as an MFM image is a convolution of both the sample and the probe's magnetic properties, it is imperative to also consider the induced effects of the probe and sample's stray-field on each other, as this can result in imaging artefacts, such as altering the moment of either the sample or the probe[35,36]. For example, Figure 2 shows the magnetic state of a low coercivity Ni disk can be perturbed by the MFM probe with higher magnetic moment (standard moment, SM) during data acquisition, compared to the low moment (LM) probe, (a and b, respectively).

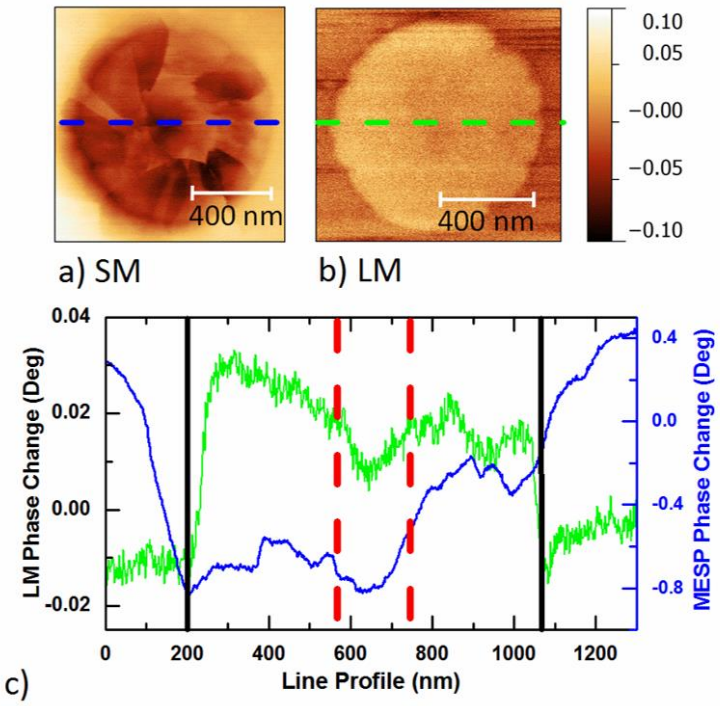

Figure 2: Imaging artefacts in MFM. MFM images of a nickel disk (diameter 800 nm and thickness 25 nm) measured with standard moment (SM) and low moment (LM) probes. The disk's magnetization is perturbed by the strong magnetic moment of the SM probe (**a**), but not by the LM probe (**b**). The line profiles (green and blue lines) were obtained with LM (left vertical scale) and SM (right vertical scale) commercial probes, respectively **(c)**. Black solid lines show the geometrical size of the Ni disk and red dashed lines mark the outline of the vortex core measured by the LM probe. Reproduced with permission from Wren *et al.*, Ultramicroscopy, **179**, 41 (2017). Copyright 2017 Elsevier.

Another common artefact in MFM data acquisition is the effects of both induced electrostatic interactions between the probe and the sample, and magnetic contamination. There are a few examples of misinterpreted MFM

images in literature due to these parasitic artefacts, including proposed magnetic highly ordered pyrolytic graphite (HOPG)[37] (demonstrated that observed contrast was due to electrostatics, i.e. not a magnetic origin, by Martinez-Martin *et al.*[38]) and room temperature ferromagnetism in C_{60} polymers[39,40] (shown to be Fe_3C contamination[41,42] and later retracted by (most) of the original authors[43]). Thus, for magnetic contamination, it is vital to carefully monitor the magnetic history and exclude exposure of magnetic materials and tools (e.g. catalysts, tweezers, etc.) to the sample in fabrication/handling processes prior to the measurement. In the case of parasitic electrostatics, it is crucial to be able to identify and nullify the adverse artefacts. For this, it is primarily important to consider the electrical grounding during the measurement, with alternative active and passive methods for nullifying the effects discussed later in Section 3.

Table I: Common limitations and errors in magnetic force microscopy

Limitation	Description	Result on MFM image	Method of compensating limitation	Rel. refs
Coupled e-static & magnetic signals	e-static, frictional and magnetic forces all influence changes in probe oscillation	Image contains contribution of all 3 signals	Kelvin probe - MFM (KPFM-MFM) Switching magnetization MFM (SM-MFM) Variable-field MFM (VF-MFM)	44–47
Sensitivity to acoustic noise, air flow & vibrations	MFM (and SPM generally) are sensitive to externally driven vibrations	Noise and artefacts due to external influences	Image processing; vacuum operation; vibration isolation tables etc.	32,48
Magnetic impurities	The probe is sensitive to artefacts, which may present on/in the sample.	False positives	Careful sample preparation, handling and measurement procedures.	49,50
Probe's stray-field distribution unknown	The exact magnetic distribution of individual probes is not known	Errors in extracting meaningful quantitative values	Modelling probe's magnetization. Probe calibration	51,52
Resolution / sensitivity balance	The active magnetic volume is proportional to sensitivity and inversely proportional to resolution	Images from small force gradients will have lower resolution. Sensitivity requires a measurable interaction force, which is proportional to the interaction volume	Resolution: Deconvolution processes; ultra-sharp probes. Sensitivity: suitable probe selection; in vacuum measurement; optimized ext. variables (T, B_{ext})	53–55
z- distance effects	At larger *z*-separations, interaction volume increases and signal strength decreases	Lower resolving power leads to errors in lateral sizes. Calibration values vary as a function of tip-sample distance.	Modelling for tip-sample distance. Controllable tip-sample distance between calibration and test samples	56,57

3. REVIEW

Here we describe the recent developments in instrumentation, quantitative MFM modelling and modern application areas of MFM. Specifically, we address such areas of instrumentational development as in-field and low/high temperature MFM, discuss compensation of electrostatic signals and energy dissipation in MFM. We also briefly present different types of MFM, i.e. dynamic magneto-electric force microscopy, bimodal MFM and magnetic scanning gate microscopy, as well as development of custom-designed MFM probes. The modern objects of MFM studies discussed here include (ultra-)thin films with perpendicular magnetic anisotropy, artificial spin ice as an example of patterned structures, magnetic topological structures, multiferroic materials and materials for Life Science applications.

a. ADVANCED MODES AND INSTRUMENTATION

Only a few years after the initial development of MFM, different groups explored the power of MFM imaging with *in situ* applied magnetic fields. Initially, custom-built approaches (typically consisting of a system of coils or permanent magnets) were implemented in commercial MFM equipment with in-plane (IP) or out-of-plane (OOP) field for maximum amplitudes ranging from 300-500 mT. At that time, hot topics included the evaluation of switching fields of sub-micron magnetic patterns[58] and the study of the magnetization reversal both in thin films with perpendicular magnetic anisotropy (PMA)[59,60] and in magnetic nanowires (NWs)[61,62] (with OOP and IP fields, respectively). As the available range of magnetic fields progressed (up to 1000 mT), it became possible to study the magnetization process in materials touted for magnetic recording media[63,64]. Specialized custom MFM systems with in field capabilities operating under extreme conditions (7 T OOP at 7.5 K and UHV) were reported, e.g. Kappenberger *et al.*[65], and used currently for probing novel nanomagnetism, e.g. exchange bias multilayers[66,67]. Moreover, the application of vector magnetic fields in MFM was recently demonstrated[21].

In addition to the standard MFM images recorded at fixed magnetic fields, two different groups developed *in situ* MFM imaging in variable field, where the probe scans along one spatial dimension, while the slow axis of the scan corresponds to a gradual change of the magnetic field[21,68]. This variable field MFM mode allows for evaluation of the critical fields in individual magnetic elements or the coercive field of the MFM probes.

The in-field MFM technique provides a reliable understanding of the internal spin structure and its magnetization reversal processes and has been recently applied to studies of both the domain configuration and domain wall (DW) properties in various magnetic thin films and nano-objects[69–71]. For example, in-field MFM has been used to characterize the novel spin configuration and the magnetization mechanism in cylindrical magnetic NWs, which are exempt of the Walker breakdown limit that restricts the DW velocity[72,73]. The in-field MFM technique is also paramount for studies of the topologically protected magnetic states characterized by the Dzyaloshinskii–Moriya interaction (DMI), e.g. magnetic skyrmions, since this technique is being intensively used to analyze their stability, nucleation and propagation[74–78].

The combination of nanomagnetism and biomedical applications has also been a hot topic in recent years, e.g. in application to studies of hyperthermia effect for cancer treatment. The study of individual magnetic nanoparticles (MNPs) by in-field MFM allows for determination of the easy axis of $Fe_{3-x}O_4$ MNPs[79,80] and the vortex state formation and annihilation in individual 25 nm MNPs[67].

Variable temperature MFM is another important topic for MFM development. Low-temperature MFM has been utilized to study superconducting flux vortices in Type II superconductors, where detailed information on the temperature and field dependence[81] of their properties can be obtained with the high spatial resolution of the MFM. Understanding phenomena such as flux creep and pinning[82] at the nanoscale is important for technological applications such as high critical temperature (high-T_c) superconducting ceramics, where creep can cause a reduction in the critical current and fields[82,83]. Low-temperature MFM measurements in the range of 7.6 – 80 K have been used to image flux vortices in $YBa_2Cu_3O_{7-x}$ (YBCO) single crystal films[84]. In these experiments, the authors employed the use of a bath cryostat with a variable temperature insert and a superconducting magnet. This system allows for measurements with a temperature range of 6 - 400 K, ultra-high vacuum and applied fields of

7 T. The same authors also demonstrated how vortex bundles can be manipulated and nucleated using the stray field from the magnet probe[85].

While piezo excitation is the most common way to excite AFM cantilevers, it is not specifically advantageous in low temperature systems, where instabilities originate from the thermal contraction of mechanical parts pressing the cantilever. In the past, the photothermal excitation of the cantilevers using two laser sources was accepted to be the best alternative method. In this one of the beams was focused at the end of the cantilever for deflection measurement, and the second beam near the base of the cantilever for excitation[86,87].

Recently a novel radiation pressure based cantilever excitation method for imaging in dynamic AFM mode was presented by Çelik *et al.*[88]. In order to simplify the optical design in cryogenic AFM/MFM, the authors explored the use of a single laser beam, and fiber optic interferometry; both for the excitation and detection of cantilever deflection in AFM imaging. The high performance of the radiation pressure excitation in AFM/MFM was demonstrated by magnetic domains in Co/Pt multilayers and an Abrikosov vortex lattice in BSCCO(2212) single crystal at 4 K[88].

In addition to low-temperature measurements, it is also possible to image magnetic phenomena and transitions that occur at higher temperatures. Typically these measurements are performed using Peltier or, for higher temperatures, resistive heaters; which can provide *in situ* measurement environments from room temperature to 520 K. It has been demonstrated that the temperature dependence of the domain structure of FePt thin films can be imaged. This is highly pertinent for future magnetic recording technologies such as heat assisted magnetic recording (HAMR)[89] where the energy required for magnetization reversal is reduced through near-field laser heating.

FeRh undergoes a first order metamagnetic phase transition from an antiferromagnet to a ferromagnet above a critical temperature of approximately 370K, which is also accompanied by an expansion of the crystal lattice and a sharp drop in the electrical resistivity[90]. It has been shown that control of the electrical resistivity in FeRh can be achieved via strain modulation of a (001) PMN-ZT piezoelectric substrate[91]. This strain modifies the relative contributions to the total electrical resistivity by modifying the relative volume of the antiferromagnetic and FM regions through the strain induced phase transition. In this work, MFM was used to investigate the first order metamagnetic phase transition of FeRh, at temperatures above and below the phase transition. It was found that the relative size of the FM domains expands rapidly through the phase transition and then reduce in size upon cooling, highlighting the effectiveness of MFM to gain insight to the magnetic landscape of complex systems on micrometric length scales.

In MFM experiments such as those already discussed, it is important to consider the electrostatic influences to the MFM signal. Here we discuss further the instrumental developments and examples relevant to separation and compensation of electrostatic signals in MFM. At typical probe–sample working distances, the magnetic and electrostatic interactions can have comparable values depending on the electric and magnetic properties of the system. An electrostatic contribution is present whenever the probe and sample exhibit different work functions, which results in a contact potential difference (CPD). Such electrostatic interaction can mask other long or short range interactions[21,92]. In a homogeneous sample, the CPD can be compensated by applying an appropriate bias

voltage between the probe and the sample. However, if the surface is composed of more than one material, this simple method is not applicable[21], since the CPD values vary all over the surface. When a heterogeneous sample (e.g. nanostructures on a substrate) is studied, and especially in the case of low magnetic moment materials, it is necessary to consider this problem in order to prevent incorrect image interpretation[37].

The first method for separating both long range interaction was proposed by Jaafar *et al.*[45]. There, a combination between Kelvin Probe Force Microscopy and MFM (KPFM/MFM) was used to distinguish between electrostatic and magnetic contributions (Fig. 1b). The method records both the CPD map and the real compensated MFM image, as it cancels the electrostatic interaction between the probe and sample at every point of the image, thus obtaining a pure magnetic signal.

Angeloni *et al.*[44] have also demonstrated the effect of electrostatic tip-sample interactions in MFM, which limited the accuracy of magnetic measurements at the nanometer scale. They developed an alternative MFM-based approach, in which the two subsequent images of the same area were collected, one with the probe being magnetized and another with a quasi-demagnetized probe. The MFM map of the true signal is achieved by subtracting the images. Prior to measurement, it is necessary to determine both the remanent saturation and coercivity of the probe by imaging a reference sample with periodically patterned magnetic domains. The authors demonstrated the effectiveness of this technique by characterizing the magnetization curves of individual MNPs[93].

The ability to distinguish magnetic and electrostatic signals is still open for discussion. Recently, it has been proposed to perform electrostatic force microscopy (EFM) prior to MFM measurements to compare the respective images[94]. Alternatively, modifying the magnetic state of the sample with an external magnetic field was used to determine whether the origin of the signal is magnetic. However, only by compensating the electrostatic interaction in each point, a true MFM image (and in addition the CPD information) can be obtained in real time[45].

Recently, a number of MFM-related techniques have appeared, each of them designed to address a specific scientific problem, thus having a somewhat narrower application scope than standard MFM. One such specialized MFM-related technique is magneto-electric force microscopy (MeFM). In this mode, the probe is not mechanically driven in the second-pass as in MFM. Instead, a combined AC/DC bias is applied to the sample whilst the sample potential is electrically modulated at the mechanical resonance of the cantilever. The resulting AC magnetic field from the sample induces resonant motion of the magnetic probe[95,96] (Fig. 1c). In addition, the probe is electrically isolated and kept at a large constant tip-sample distance during imaging[35]. This method is of particular importance for materials exhibiting a strong coupling and interdependence of electrical and magnetic properties and can be employed to detect the electric field-induced magnetization.

MeFM has been used previously to: decouple magnetic and electrical effects in complex samples (e.g. 2D electronic liquids[35]); visualize the magnetoelectric (ME) response from domain patterns in hexagonal manganites[95,96] and antiferromagnetic 180° domains[97]; and estimate the upper limit of the linear ME coefficient of *h*-$LuFeO_3$[98]. Additionally, many controlled experiments have been undertaken, e.g. a study of MeFM performance in dependence on the modulation frequency[96], which showed that lower modulation frequency produces a better signal-to-noise ratio (SNR). However, lower modulation frequency requires longer averaging time to obtain the intrinsic ME response.

Superior aspects and limitations of MeFM were recently summarized by Schöenherr *et al.*[97]. The advantages include: i) high lateral resolution with standard/specially formed probes; ii) ability to resolve and define the DW inclination; iii) low sensitivity to material inhomogeneities and thus reduced dependence on the associated scattering effect. The current restrictions of MeFM are a relatively small output response and low SNR. Nevertheless, the limited signal can be improved by: increasing the electric field, resulting in a larger induced magnetic field; optimizing the temperature to maximize the ME effect response; optimizing the electrodes; use of probes with higher magnetic moments, leading to a stronger force between the probe and the magnetoelectrically induced magnetic field. The SNR can also be improved by increasing the averaging time per data point or multiple measurements of the same area. It was thus compellingly demonstrated that this advanced technique provides direct visualization of the ME domains and DWs to open up a new paradigm of explorations of emergent mesoscopic phenomena in materials with multiple coupled orders. It was proposed that the method is of utmost importance for exploring emergent phenomena at the mesoscopic scale such as ME coupling in multiferroic domains and DWs, multiferroic skyrmions or magnetic topological insulators.

Bimodal MFM belongs to the family of multi-frequency SPM. One of the advantages of SPM is the simultaneous detection of a variety of interactions at different probe-sample separations. Multi-frequency SPM is a novel concept that has been developed in the last few years[99]. These modes are based on the consideration of the microcantilever-based probe as a mechanical system characterized by multiple resonances and harmonics. Each of those frequencies are sensitive to specific information on the sample properties. Appropriately excited and decoded, those frequencies will provide complete information on the electronic and mechanical properties (Fig. 1d).

For the particular case of MFM, the multi-frequency techniques have become an active area of research. In 2009, Li *et al.* presented the bimodal AFM as a technique to simultaneously separate short- and long-range (topographic and magnetic, respectively) forces in ferromagnetic samples[100]. In this work, the cantilever was driven at two flexural resonant modes. Following this idea, Dietz *et al.* employed the bimodal AFM to measure a nanomechanical effect that enables the detection of ferritin molecules with high lateral resolution and sensitivity[101]. More recently, a non-contact bimodal MFM technique operating in vacuum/UHV was developed[102]. In this work, the higher-stiffness second mode is used to map the topography and the magnetic force is measured at first oscillation mode, which is characterized by higher sensitivity. The torsional resonance mode of cantilever oscillation was employed to performed magnetic imaging without topography-related interference and to improve the lateral resolution[103].

Another alternative is to combine a mechanical (1st mode) and electrical excitation (2nd mode) to drive a cantilever. This approach has been explored in the literature to separate electrostatic and magnetic interactions [38,45] or as a tool to control the probe–sample distance[31,104]. In a similar way, in the secondary resonance MFM (SR-MFM) the excitation of the probe is bimodal: the information from the first eigenmode (mechanically excited) is used to obtain the topography but the higher eigenmode is excited by an external magnetic field instead of the piezo. The long-range magnetic forces are separated from short-range allowing a single-pass imaging of topography and magnetic images with high sensitivity, which makes this bimodal MFM technique a useful tool for the characterization of samples with weak magnetic properties[105].

Another powerful tool for probing physical phenomena in an MFM-related technique is the study energy dissipation. In SPM, the dissipation of energy is evaluated by measuring variations in the cantilever oscillation[106]. For MFM, the pioneering work[107] uses these dissipative maps to distinguish between Néel and Bloch DWs or identify pinning sites. It has since been demonstrated that some instrumental artefacts can affect the measured values[108].

Classical magnetic dissipation force microscopy (MDFM) studies probe-induced magnetization changes in the sample, but recently the opposite effects has also been studied: the strong probe–sample interaction where the stray field from the sample induces changes in the magnetic state of the probe (Fig 3a). Iglesias–Freire *et al.*[109] demonstrated that the magnetic switching at the apex of an MFM probe can produce artefacts in MFM images, and could be misinterpreted as a true signal. The authors used this effect to obtain a 3D map of the sample stray field (Fig. 3b). More recently, Jaafar *et al.*[110] discussed a counterintuitive behavior of energy dissipation with probe–sample distance for domains with magnetic moments parallel to the probe's magnetization. Thus for a large range of distances, the probe-sample separation is directly proportional to the probe's oscillatory excitation energy. The recorded dissipation values (~fW) were in good agreement with micromagnetic calculations, corresponding to the power losses caused by relatively small regions of spins switching their magnetization. A high spatial resolution (<8 nm) was achieved in the MDFM images; thus, MDFM has been demonstrated to be a promising technique for MNP characterization[109,111].

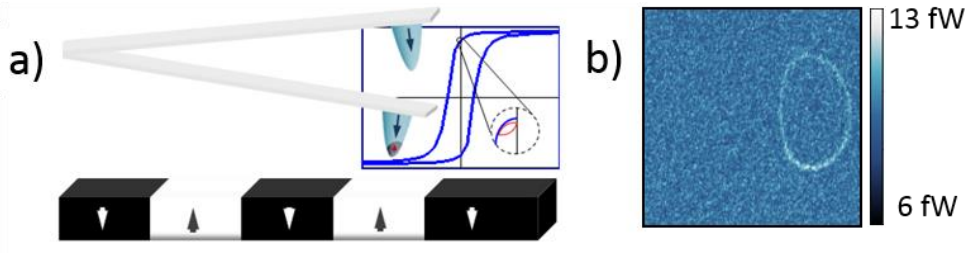

Figure 3: Magnetic dissipative force microscopy. (a) Sketch of the dissipation process associated to the variation of the stray field from the sample due to the interaction with the probe. **(b)** Magnetic dissipation image corresponding to a Py dot under in plane applied field of 60 mT. Reproduced with permission from Iglesias-Freire *et al*., Appl. Phys. Lett., **102**, 022417 (2013). Copyright 2017 AIP Publishing.

As MDFM requires a strong probe-sample interaction, which can be a limitation when measuring in high vacuum, Zhao *et al.*[31] developed a frequency-modulated capacitive-distance control method, which is valid even in the presence of energy dissipative processes. Another proposed approach for mapping energy dissipation is using drive amplitude modulation AFM (DAM-AFM)[112]. The method uses the monotonicity of the dissipation force between the probe and the sample to obtain stable images in all environments (e.g. vacuum or liquid suspension)[24]. In DAM-AFM, the topography map is obtained by using the dissipation of energy as the feedback parameter while the frequency shift, controlled by the phase-locked loop, provides information about the conservative interactions.

Magnetic scanning gate microscopy (mSGM), also known as magnetoresistive sensitivity mapping, modifies the electrical properties of a device under applied voltage in proximity of the scanning MFM probe due to magnetoresistive effects (Fig. 4). From the applied potential difference across the device, electrostatic interactions

between the probe and the sample heavily influence the acquired data. Thus, mSGM is often combined with KPFM similar to the KPFM/MFM technique.

The modulated potential difference, induced by magnetoresistive effects from the probe-sample interaction, can be mapped by locking into the frequency of the MFM probe's oscillation across the device with a lock-in amplifier. Hence, the noise generated by the frequencies of the sidebands (from bias modulation on the probe) or the scan rate of the probe across the sample can be removed, allowing for faster data-acquisition and greater SNR.

In the past, mSGM has been used to characterize giant magnetoresistance (GMR) sensors and obtain sensitivity maps to external magnetic fields. In particular, it has been applied extensively to characterize hard disk drive reading heads[113,114]. Recently, it has been used for characterization of L-shape permalloy (Py) devices[115,116] and measure the probe stray field using graphene Hall sensors[117–119]. For the former example, devices with pinned DWs were scanned using non-magnetic probes modified with a magnetic bead[116]. By monitoring the resistance across the device, it is possible to estimate its sensing volume towards a specific magnetic bead (or any other nanostructure on the probe). This approach enables testing many devices with the same magnetic bead and thus allows correlating results for optimization of the sensing elements. Other recent developments include: using the probe's stray field to manipulate DWs; measuring electrical signals originating from the anomalous Nernst and Hall effects as a way of sensing the position of the DW inside of the nanostructure[120,121] and writing magnetic landscapes with thermal assistance for magnonic devices[122].

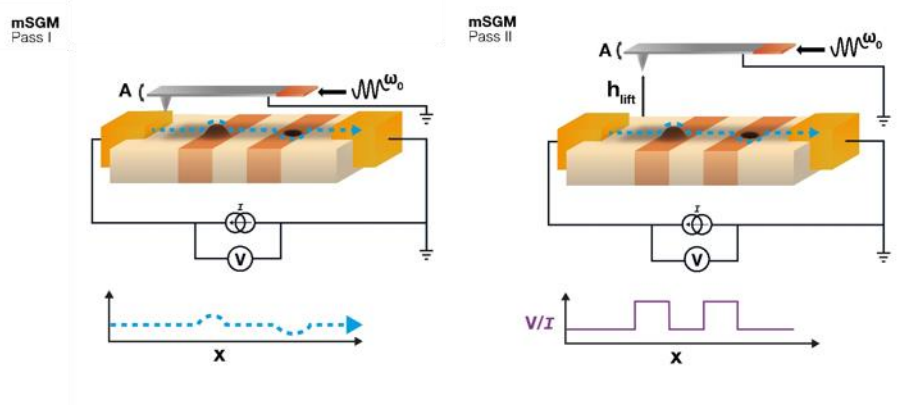

Figure 4: Schematics of magnetic scanning gate microscopy. An electrically connected, current-biased device, is scanned by a magnetically coated probe, and the transverse voltage response at the resonant frequency of the probe is recorded as a function of the probe's position. Typically this technique is combined with FM-KPFM, as the applied current gives rise to electrostatic artefacts.

Custom-made MFM probes have been developed to improve the lateral resolution and sensitivity beyond the limit of commercial MFM probes and also to facilitate quantitative MFM (qMFM) studies, e.g. by increasing/reducing the coercive field, or modifying the stray field distribution and intensity (Fig. 5). Three trends can be primarily identified: (i) customized *magnetic coatings*, where the magnetic properties of the material are varied; (ii) probes with magnetic *adhered structures*, such as Fe-filled carbon nanotubes (CNTs) or magnetic beads; and (iii) MFM probes with *fabricated nanostructures*.

Among these three approaches, modifying the *magnetic coatings* of an MFM probe is the most common as it does not require extensive nanofabrication capabilities[119,123,124]. Such probes are characterized by the enhancement

of the lateral resolution both in the topography and in the phase/frequency shift signal. This has been achieved, for instance, by partially coating MFM probes[123,125], or depositing multiple layers of magnetic material to be able to control high/low moment states and if necessary limit the eminent stray-field to the probe's apex[119,126]. The other advantage of customized magnetic coating is a possibility to match the magnetic properties of the probe to that of the sample. For example, reducing the stray field produced by the probe reduces its interaction with soft samples, or conversely increasing the coercivity of the probe helps to image samples with strong stray fields.

A different approach is to *adhere magnetic structures* to the apex of a non-magnetic probe, which was in many cases used in attempt to create a dipole-like [116,127–129] or monopole-like probe[130]. CNTs filled or coated with magnetic material have been attached to the apex of standard AFM/MFM probes[131,132] to improve the lateral resolution of the MFM (Fig. 5a). However, this approach is usually at the cost of the sensitivity, due to the small amount of magnetic material interacting with the sample. Another alternative is attaching microscopic pieces of hard magnetic material[133] or magnetic beads[116,127–129,134,135] (Fig. 5b and c, respectively) to the probe apex. In both cases, the typical size (~1 μm) is far larger than a probe's apex diameter (~30 nm), which could jeopardize the lateral resolution.

The ability to *fabricate nanostructures* on the probe apex opens the possibility for engineering the magnetic properties by selecting the coating material, but also to use shape anisotropy as a way of governing magnetization. The most common approach consists of using electrical current to induce chemical deposition and hence achieve a sharp apex[136,137]. However, the sharpness of the apex may vary from probe to probe. Another approach uses focused ion beam (FIB) milling to sharpen probes into a needle with magnetic coating only at the very end of the needle[25,138] (Fig. 5d). This approach has the advantage of producing sharp probes with high lateral resolution, but with small magnetic moment. The last type of custom-made probes consists of nanostructures built at the probe's apex to use shape anisotropy to constrain the magnetization and produce a strong stray field just. For example, a V-shaped magnetic nanostructure fabricated on one face of a non-magnetic probe was recently demonstrated (Fig. 5e). Such probes combine a low moment with high coercivity to reduce magnetic switching in the presence of strong stray fields[36]. A very recent work[139] combines all three strategies by first developing a hard magnetic thin film architecture most suitable for MFM on an appropriate flat substrate (i), creating a nanostructure (slim triangular needle) from the substrate film compound by FIB (iii) and adhering this nanostructure to a non-magnetic cantilever (ii). In the above work a high resolution MFM probe with unrivaled coercivity and thus stability against large magnetic fields has been fabricated from a $SmCo_5$ film grown epitaxially on MgO.

MFM probe characterization is a fundamental part of the MFM experiments and particularly relevant for qMFM and in-field MFM. When assessing the suitability of an MFM probe for an application, it is recommended to consider: its geometry (e.g. by SEM)[119,121,140]; its coercive field (e.g. from in-field MFM)[131,141]; and its magnetization profile (e.g. by electron holography[119,121,140], measurement of a reference material[36,130,142], or Hall sensors[118,119,143–145]).

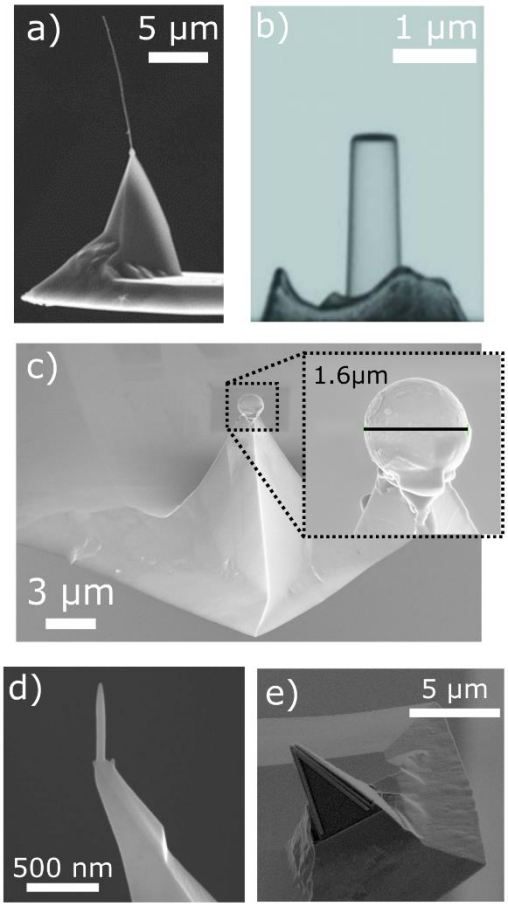

Figure 5: Examples of custom MFM probes. a) Probe with a carbon nanotube filled with magnetic material. Reproduced with permission from Wolny *et al.*, J. Appl. Phys., **108**, 1 (2010). Copyright 2010 AIP Publishing. **b)** Probe with a magnetic disk on top of a FIB milled cylinder. Reproduced with permission from Amos *et al.*, J. Appl. Phys. **105**, 07D526 (2009). Copyright 2009 AIP Publishing. **c)** Probe with a magnetic bead attached. Reproduced with permission from Corte-León *et al.*, J. Magn. Magn. Mater. **400**, 225–229 (2016). Copyright 2016 Elsevier. **d)** FIB sharpened probe. Reproduced with permission from Belova *et al.*, Rev. Sci. Instrum. **83**, 93711 (2012). Copyright 2012 AIP Publishing. **e)** Probe with a lithographically patterned V-shaped nanostructure on one of the sides. Reproduced with permission from Puttock *et al.*, IEEE Trans. Magn. **53**, 1–5 (2017). Copyright 2017 IEEE.

b. QUANTITATIVE MFM MODELLING

Different approaches to qMFM have been developed in the past two decades, which provide a quantitative description of the magnetic probe. They range from simple point probe approximations (PPA)[57] to geometrical probe descriptions[146] and finally to parameter-free tip transfer function (TTF) methods[25,52]. All approaches start from the correct magnetostatic interaction between the probe's magnetization and the sample's stray field but use various degrees of simplification. For a linear oscillation regime and a negligible cantilever tilt, in the most general description, $\Delta\phi$ is calculated without any restrictions on the magnetization structure $\overrightarrow{M_t}(\overrightarrow{r'})$ within the probe as:

$$\Delta\phi \sim \frac{\partial F_z}{\partial z} = \frac{\partial^2}{\partial z^2} \iiint_{V_{tip}} \overrightarrow{M_t}(\overrightarrow{r'}) \cdot \overrightarrow{H_s}(\vec{r} + \overrightarrow{r'}) dr'^3 \qquad [11]$$

Geometrical models often assume a simplified magnetization structure for the probe, e.g. $\overrightarrow{M_t}(\overrightarrow{r'}) = M_{z,t}$, but attempt a realistic expression for its shape and volume. Equation [11] thus reduces to:

$$\Delta\phi \sim M_{z,t} \iiint_{V_{tip}} \frac{\partial^2}{\partial z^2} \cdot H_{z,s}\left(\vec{r} + \overrightarrow{r'}\right) dr'^3 \qquad [12]$$

In the PPA models, the magnetization is assumed to be concentrated in one point within the magnetic probe. In case of the point dipole approximation, equation [12] thus further simplifies to:

$$\Delta\phi \sim m_z \cdot \frac{\partial^2 H_{z,s}\left(\vec{r}+\vec{\delta}\right)}{\partial z^2} \qquad [13]$$

Here, $\vec{\delta}$ describes the position within the tip, where the dipole moment m_z is supposed to be located.

This disregards an important aspect of the magnetostatic interaction: the interaction volume of a realistic 3D probe with the stray field of the sample $\overrightarrow{H_s}$ will depend on the size and morphology of the measured domains. Thus, PPA models should be applied only to samples with regular stray field patterns. Recent works report on the moment quantification in laterally confined objects such as MNPs[93,147–149], chains of magnetosomes[150] or patches of single molecular magnets (SMM)[151]. In most cases, the tip's point-probe parameters were freely adjusted to allow a self-consistent data description, but not determined from an independent sample. On the other hand, quantifying the signal of an individual nanoscale object is not easily done with other methods. Uhlig *et al.*[127] made use of the point probe character of an MNP by picking up such a particle with a non-magnetic probe. By preparing such an MFM probe the PPA model description is more justified than for volume probes.

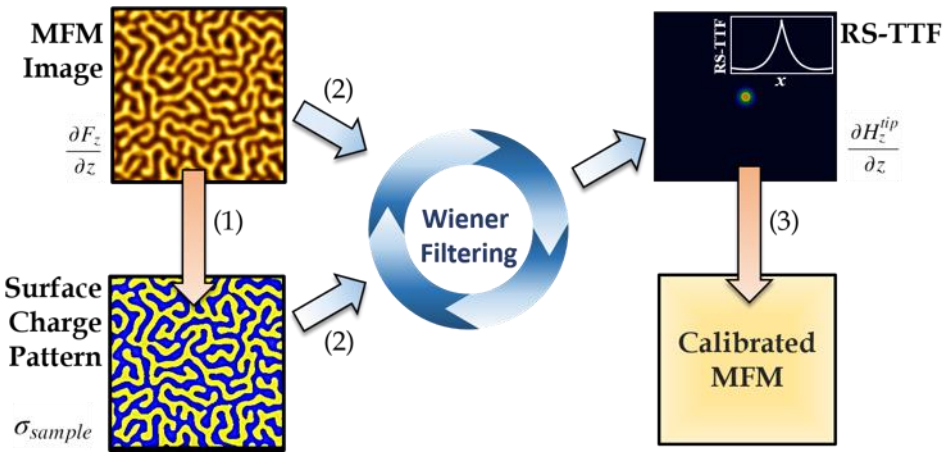

Figure 6: Schematics for image-processing steps to acquire the real-space tip-transfer function (RS-TTF). The "real" MFM image (top left) is used to generate an effective surface charge pattern (bottom left) by binarizing the image and adding in magnetic or experimental parameters (i.e. DW-width, lever-canting, and M_s). The two images are deconvolved in Fourier space by means of Wiener filtering to produce the stray-field derivative of the probe (top right). This can subsequently be used to produce calibrated/quantitative MFM measurements, as it can be deconvolved from the MFM image of a sample with unknown magnetic parameters.

The TTF approach by Hug *et al.*[25] calculates the force on an MFM probe exerted by the stray field of a sample with perpendicular magnetization in Fourier space (Fig. 6). By means of a calibration measurement of a suitable reference sample, one derives a model-independent and parameter-free description of the probe's imaging properties. Considering that even nominally identical probes (from the same manufacturer/batch) can result in

large variance of the MFM contrast on an identical sample, this experimentally more elaborate approach is thus judged to be of great importance. The researchers have successfully applied this approach to experimental means, e.g. for the quantification of non-compensated moments in exchange-bias systems[152]. Neu *et al.* have followed this qMFM approach for, e.g., identifying the vortex state in a magnetic nanowire[54], calibrating custom-made probes[119], or quantifying the stray field in the corner of an L-shaped Py structure[36]. A recent application of qMFM quantifies artificially patterned stray field landscapes in CoFe/MnIr exchange bias layer systems[153]. Although successful, this study also reveals the difficulties that arise with the quantification of a complex multiscale domain pattern. Reference samples and measurements need to cover a large range of spatial frequencies to correctly calibrate the probe for all relevant length scales. Due to the even larger complexity and multi-scale character of magnetic domains present in modern permanent magnets[154], qMFM measurements have not yet been performed on this important set of materials, although it is expected that highly resolving and quantitative MFM measurements can lead to a large improvement of their understanding.

c. MODERN OBJECTS OF MFM STUDIES

In this part, we discuss applications of MFM and the relevant daughter techniques to modern areas of the physics and the material science. It is noteworthy that such applications are very often quite challenging, dealing with extremely low magnetic signals and requires the ability to distinguish the magnetic response from the other components (i.e. electrostatic contributions, magnetic contaminations, etc.).

We start this part of the Review from considering applications of MFM to thin films with PMA. The interpretation of MFM images is most straightforward for samples with a magnetization orientation perpendicular to the imaged surface. Here, the stray fields produce a qualitative MFM contrast to closely resemble the underlying domain structure. Hence, a wealth of MFM studies focus on the imaging and interpretation of films with PMA, quantified by the (perpendicular) uniaxial anisotropy constant K_u. In the case of large PMA (ideally $K_u >> K_d = ½\mu_0 M_s^2$), these band domains can be approximated as being homogeneously magnetized along the *z*-axis (colloquially up or down), forming a domain morphology that depends among others on field history, surface corrugation and coercivity. Domain theory of such high PMA films is well established and the knowledge of M_s, K_u and the DW profile allows a correct quantitative reconstruction of the magnetic domain pattern (or, equivalently, the effective magnetic surface charge pattern) from a qualitative image. Thus, such films are well-suited as reference samples for probe calibration (see section 3b).

Recent MFM work on films with PMA can be roughly segregated into the following four groups. The first deals with films with large PMA, where the equilibrium domain width can be used to judge the balance between the various energy terms. For thin film systems with DMI, such comparisons between domain theory and observed domain widths gathered great importance to conclude on the less accessible DW energy[155].

The second group considers films with smaller PMA (i.e. $K_u < K_d$), where the dominating shape anisotropy pulls the magnetization vector into the film plane, but still the presence of PMA can lead to a modulation of the magnetization vector perpendicular the surface. These stripe domains are again observable by MFM but the magnetization possesses a complex depth dependent structure, which can only be approximated by analytical theory and otherwise requires micromagnetic calculations. A recent work demonstrates the influence of the weak

PMA on the domain structure in soft magnetic $NdCo_5$ films with anti-dot structure[156]. Evaluating stripe domain patterns in a quantitative way has so far not been accomplished to satisfaction. This is due to the lack of qMFM studies and the difficulties in theoretically describing the magnetization pattern.

The third group includes samples, in which a layer with PMA is exchange-coupled to a soft layer with in-plane magnetization, which are a subject of recent studies to obtain a microscopic view of how exchange-coupling occurs in layers with orthogonal anisotropies, see e.g. an example on the [Co/Pd]/Py system in Ref. [157]. The final group includes laser-induced manipulation of a sample's magnetization state, which can be imaged with high resolution by MFM and may give insight into the origin of loss and sometimes also re-entrance of magnetic order[158].

Beyond thin-films, another highly researched topic of study is patterned magnetic media. Patterning FM materials into novel shapes and structures are of particular interest in applications such as logic devices or novel magnetic recording[159]. As methods for patterning materials on the nanoscale improve, as they have been consistently, ways to characterize the new synthetic designs are required to measure the exotic and useful properties they possess. MFM previously has been highlighted as an important tool for understanding the magnetism within such structures, ranging from memory devices (e.g. bit-patterned media)[159] to magnetic strips, and nanodot and antidot arrays[160–163]. One of many modern examples of magnetic patterned structures that are popularly researched are artificial spin ice (ASI), which exhibit geometric frustration, ordering of effective magnetic charges, and a variety of collective dynamics[164–166].

ASI consists of lithographically patterned arrays of nanoislands/NWs of different designs composed of in-plane FM material, which are magnetically frustrated due to the intrinsic geometric ordering to create two out-of-plane Ising-spins for each nanoisland[167–169]. ASI have received attention as the frustrated arrays can be controllably pinned into multiple stable/meta-stable states, priming them for magnetic recording, logic devices and experimental hot-beds for understanding magnetic frustration in more complex systems. In their ground-state some of the most popular structures in literature [e.g. squares and honeycomb lattices (Figure 7 a-b and c-d, respectively)] obey the ice-rule[167], but can be excited into higher energy states by external stimuli (e.g. by applied field). Wang *et al.*[170] demonstrated reading, writing and erasing of individual bits by applying in-plane field below the nanoisland saturation-field and individually switching nanoislands with an MFM probe, demonstrating great precision for single bit writing. Gartside *et al.* [171] similarly introduced topological defect-driven magnetic writing on ASI using the MFM.

Another extremely interesting example of recent objects of MFM studies are magnetic topological structures. Topological solitons, or defects, in magnetic materials have provided, and continue to provide, a rich plethora of phenomena to be studied for fundamental research[66,172–174] and future magnetic based technologies[175], which rely on various novel magnetic configurations and architectures. Typically, these defects in magnetic materials are manifested as magnetic domain-walls[176,177], vortices[178–183], skyrmions[184,185] or magnetic bubbles[186]. Here, we focus solely on the use of MFM in observing and quantifying physical phenomena occurring in DWs and vortices. MFM studies of skyrmions will be discussed in the Perspective section (section 4c).

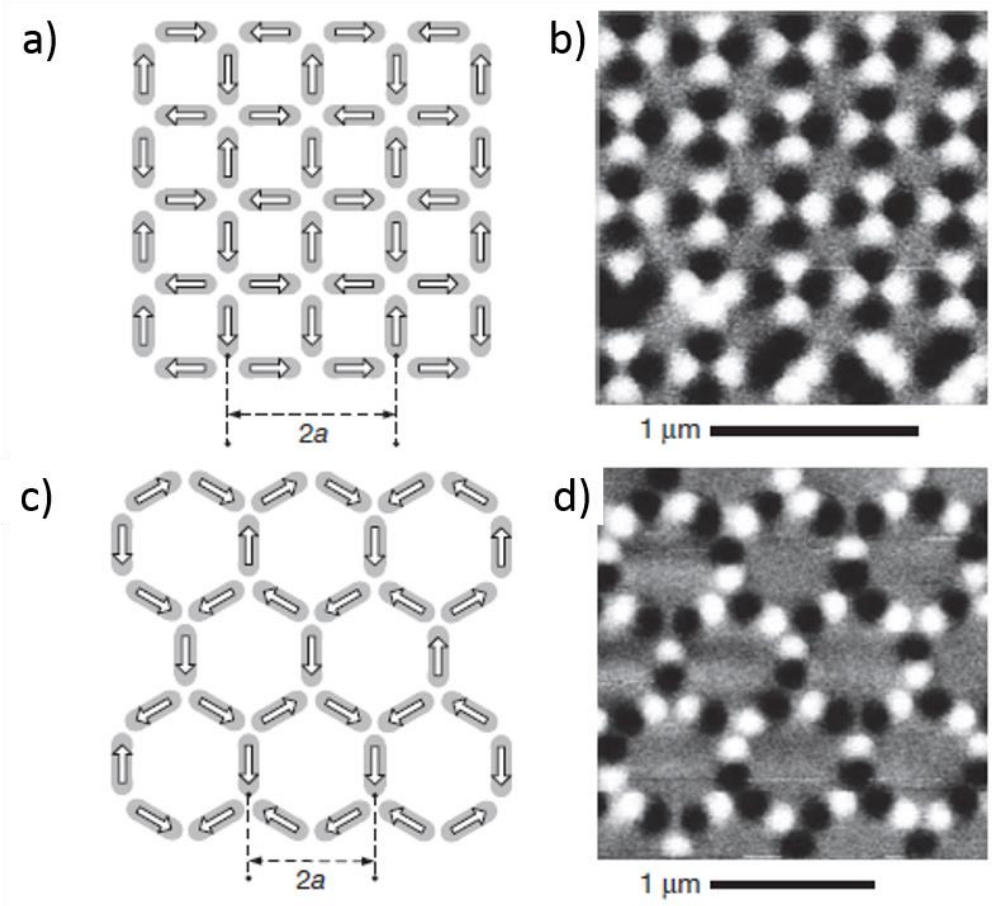

Figure 7: Artificial spin ice. Illustrations of the nanomagnet configurations used to create artificial square (a) and kagome (c) spin ice, and their corresponding MFM images (b and d, respectively). The black and white spots correspond to the magnetic poles of the islands. The arrows in (a) and (c) correspond to the magnetic moments revealed by the corresponding MFM images. *a* indicates the lattice constant. Reproduced with permission from Zhang *et al.*, Nature Letters, **500**, 553 (2013). Copyright 2013 Springer Nature.

Magnetic domains and the walls that divide them are determined by the subtle balance of the following main contributions of micromagnetic energy: exchange interaction, magnetostatic and magnetocrystalline energies[177]. Understanding DW motion and dynamics under the influence of an applied stimulus such as magnetic field or spin polarized current pulses can elucidate to the complex underlying magnetization reversal processes and how DWs can be manipulated for use in modern technologies. Here, MFM excels as a tool to investigate phenomena such as the domain structure in magnetic nano-patterned elements following the application of an external stimulus in so-called quasi-static measurements. This is of high importance for technological applications of DWs[187] such as that of the racetrack memory (RM)[175]. RM offers a significant gain over conventional magnetic storage devices and potential silicon based logic circuitry in terms of performance[188]. Here, spin polarized currents are used to generate spin torque transfer (STT)[189,190] such that DWs in the racetrack can be moved along a track, which extends into the third dimension[175,191] increasing the effective bit density. Recent developments have moved to more exotic phenomena to drive domain-wall motion where spin-orbit torque (SOT) effects, such as the Rashba effect[192,193] and the spin Hall effect[194,195].

MFM is often also used to investigate complex domain type structures where the geometry, hence the magnetostatic energy, of the material system starts to play a dominant role [196–198]. This alters the equilibrium

configuration such that it becomes more complex than in the typical cases of Bloch or Néel type DWs in thin films. Examples of these wall types include the transverse/asymmetric transverse DWs[196,197,199] and single, as well as multiple, vortex walls[196,197,200]. Understanding the internal structure of such DW configurations is important not only for scientific interest but also for applications as the internal structure strongly dictates the DW dynamics[174]. Recently, Nguyen *et al*. have demonstrated that in Py nanostrips with in plane magnetization a so-called Landau DW exists[174]. This novel DW configuration is described as a flux closure pattern that resembles a Landau pattern, however, it is elongated and encircles a Bloch type wall. In this work, MFM was integral in confirming the predicted domain configurations obtained by employing finite difference methods to solve the Landau–Lifshitz–Gilbert equation[201].

Of particular interest is the case of cylindrical wire and FM nanotube type geometries. Arrays of such wires have potential in many advance technological areas, including data storage and information, energy, Life Science and environmental sectors[202]. Furthermore, numerical simulations have predicted that the Walker breakdown limit in such 1D nanostructures is topologically forbidden[203], making them extremely attractive for technological applications requiring DW displacement. In these geometries, a number of topological defects can be identified: transverse DWs; asymmetric transverse DWs; and Bloch point walls, which are similar in nature to vortex walls found in FM nanotubes[204]. Due to its high spatial resolution and sensitivity MFM has been widely used to study the domain configurations of such wires. For example, it has been shown that in Co NWs of dimensions 45 nm in diameter and 10 μm in length an alternating pattern of vortex states is energetically favorable, offering an interesting route towards novel spintronic memory devices[205]. Similarly, the spin configuration has also been investigated in Co bamboo-like NWs with diameter modulation[202]. Using MFM it was demonstrated that, due to the competition between the magnetocrystalline and shape anisotropy energies, multi-vortex structures with alternating chirality form. Interestingly, as it was evidenced by MFM data, DW pinning in the modulated diameters wires was avoided, in contrast to other materials (FeCuCo) investigated in the same study.

In addition to DWs in thin films and nanowire type topographies, confinement in nano-sized patterned elements can lead to stabilization of vortex cores[179]. These are of particular interest due to the potential they hold for future microwave sources magnetic sensors and logic as well as in non-volatile memory applications[206]. Vortex cores exist as a thermally stable flux domain pattern that can be typically characterized by in plane winding of the magnetization around a perpendicularly magnetized core[182]. Vortex cores, which can be as small as 10 nm[181] in size, possess polarity ±p with respect the out-of-the-plane axis and a given chirality. MFM has proved an invaluable tool for the investigation of vortex cores and indeed was used in the first observations of vortex cores in patterned disks of Py[178]. Additionally, MFM has been utilized to explore the switching of vortex cores using current driven vortex excitation via spin torque transfer[180] paving the way for electrical control of magnetization in logic devices.

Multiferroics is another modern class of materials where MFM and MeFM are used, often in conjunction with piezo force microscopy (PFM) studies. The coupling between the magnetic and electric dipoles in multiferroics holds a vast promise for conceptually novel electronic devices and has been widely explored in the last decade. The ME phenomena have a profound and broad impact on diverse areas of materials science from multiferroic materials to topological insulators, where direct visualization of ME domains and DWs is of both fundamental

and practical importance. Specifically, MFM has been proven as an essential technique for studies of multiferroic (in particular, ME) materials that exploits both FM and ferroelectric (FE) properties.

MFM is typically used to reveal the microstructure of both single-phased multiferroics and multiferroic composites, such as detection of the strong magnetic contrast, visualization of the magnetic structure of grain boundaries, and reviewing the appearance of non-magnetic pores between the phases in nanostructured ME materials[207]. MFM imaging was used to reveal the presence of magnetic domains being extended over several adjacent ferrite grains in $BaTiO_3(Ni_{0.5}Zn_{0.5})Fe_2O_4$ multiferroics[208] and in $BiFeO_3$ NWs[209]. In many cases, it was advantageous to use extended modes of MFM, i.e. in-field MFM or under the action of electrical poling.

Additionally, MFM was used to establish the nature and overall contribution of the material properties originating from magnetic and multiferroic defects. In the relaxor FE single-phase $(BiFe_{0.9}Co_{0.1}\ O_3)_{0.4} - (Bi_{1/2}K_{1/2}TiO_3)_{0.6}$, $CoFe_2O_4$ magnetic clusters with sizes 0.5–1.5 μm were identified using MFM[210]. Such inclusions exhibit only a magnetic dipolar response, indicating magnetization along the in-plane orientation. On the other hand, a combination of MFM and PFM showed that multiferroic clusters (unspecified in nature) exhibit both FE and strong magnetic properties. It is expected that these findings will lead to new research in this novel class of non-ergodic relaxor multiferroics, especially as the material is Pb-free and consists only of abundant elements[210]. The overall concept is ideal for an electrically controlled magnetic nanodot storage device[211].

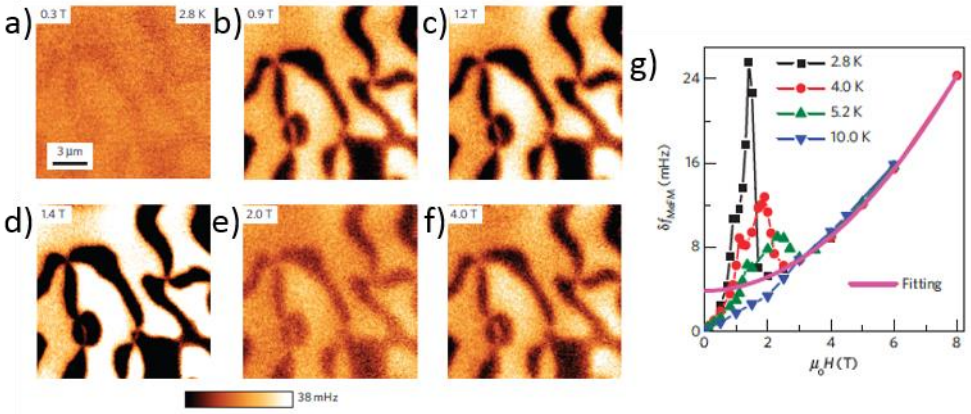

Figure 8: MeFM images and the magnetic field dependence of the MeFM signal. (**a–f)** The representative MeFM images taken at 2.8K in various magnetic fields. All of the images are in the same color scale. **(g)** Field dependence of the MeFM signal at 2.8, 4.0, 5.2 and 10 K, respectively. For details, see Ref.[95]. Reproduced with permission from Geng *et al.*, Nature Materials, **13**, 2 (2013). Copyright 2013 Springer Nature.

Local MFM studies were used to directly demonstrate magnetization reversal under purely electrical control in another $BaTiO_3$/Ni system, which is the outstanding goal in magnetoelectrics[212]. The authors primarily used MFM to study a commercially manufactured multilayer capacitor that displays strain-mediated coupling between magnetostrictive Ni electrodes and piezoelectric $BaTiO_3$-based dielectric layers. The authors evidenced that the anisotropy field responsible for the perpendicular magnetization could repeatedly be reversed by the electrically-driven magnetic switching. Demonstration of non-volatile magnetic switching via volatile FE switching was used to inspire the design of fatigue-free devices for electric-write magnetic-read data storage[212].

Direct visualization of ME domains in multiferroics was demonstrated using low temperature *in situ* MeFM from lock-in detection of electrically-induced magnetization. The authors directly demonstrated the local intrinsic ME response of multiferroic domains in hexagonal $ErMnO_3$[95] and $YbMnO_3$[96], distinguishing contribution of six degenerate states of the crystal lattice, which are locked to both FE and magnetic DWs. Results were in excellent agreement with the symmetry analysis, and a giant enhancement of the ME response was observed in proximity of the critical temperature. This suggests that critical fluctuations of competing orders may be harnessed for colossal electrically-induced magnetic responses (Fig. 8). The use of cryogenic in-field MFM was also demonstrated by Wang *et al.*[98]. Labyrinth-like domains (~1.8 μm) in an *h*-$LuFeO_3$ thin film were observed after zero-field cooling below the Néel temperature, $T_N \approx 147$ K, where weak FM order with a canted moment exists. At 6 K, MFM images of the magnetization reversal process reveal a typical domain behavior of a pinning-dominated hard magnet. The temperature dependence of the domain contrast demonstrates that MFM is able to detect the domain contrast of magnets with miniscule magnetic moments (~0.002 μ_B/f.u.).

Moving away from traditional applications in physics and material science, MFM has lately gained a momentum for studies of magnetic nanomaterials for Life Science applications. There is a broad range of applications using magnetic beads and MNPs, including cell separation, bio-sensing, *in vivo* imaging, magneto-thermal therapy, etc.[213,214] Alternatively, the use of elongated nanostructures such as magnetic cylindrical NWs is of a growing interest in different bio-magnetics applications due to their high aspect ratio, anisotropic physical properties and the possibility to work with different length scales[215].

A direct characterization of the magnetic properties of individual beads and MNPs on nanoscale is possible by microscopy-based techniques such as MFM. For example, MFM has recently been used to detect superparamagnetic and low-coercivity[79,80,148,216,217] MNPs. Also, MFM has been successfully employed to characterize MNPs inside biological systems as vesicles (niosomes)[218], virus-capsids[219] or cells[220], where MFM images were used to evaluate the amount of magnetic material inside the different entities.

In addition, MFM has been used to investigate the magnetic properties of individual NWs[221] and vortex-state dots[163] for biomedical applications. Molecules, such as ferritin, have also been characterized by liquid-MFM[222,223]. However, it is crucial to remember that MFM is sensitive to non-magnetic (e.g. electrostatic) signals (see Section 3a)[44], especially in the case of biological systems, where the strength of the produced stray field are near the sensitivity limit of the technique.

In the case of biological systems it is essential to perform sample characterization in relevant environmental conditions, e.g. physiological environment. For that reason, non-standard methods such as bimodal[101], energy dissipation[111] or AC-field modulated MFM[224,225] have been explored in recent years. Another approach is the use of custom magnetic probes specifically designed for biological applications[123,226]. However, since MFM has historically been applied to the study of inorganic materials, the potential of MFM for biological/biomedical applications is still under development[227]. The recent studies have demonstrated essential MFM capabilities (i.e. high enough lateral resolution and sensitivity) for studies of individual MNPs in a liquid environment[24]. This development opens new possibilities of studying magnetic systems in biologically relevant conditions.

4. PERSPECTIVE OUTLOOK FOR MFM

The Perspective part of the paper presents the emerging trends in the field of MFM concerning further development of instrumentation (e.g. in combination with other SPM modes and radiation techniques), the wider applications of qMFM measurements, and application of MFM and its sister modes to studies of advanced and emerging materials.

a. NOVEL AND MULTIFUNCTIONAL INSTRUMENTATION

The MFM community incorporates a variety of users: from beginners that demand a friendly and reliable interface to the highly specialized researchers that customize or even build their own system. It should not be forgotten that the majority of the commercial MFM users are interested in pushing the resolution and sensitivity limits of the technique. While commercial, off-the-shelf systems still remain a valid indispensable tool for a routine inspection of magnetic properties of samples, modern challenges in both research and industry demand development of new advanced MFM modes. To fulfil this need the current research is targeted in different directions, including development of a new MFM instrumentation and flexible software, novel types of MFM probes (a key point still under development), and combination of MFM with other techniques targeting complex material properties, which is a general trend to make the MFM compatible with the simultaneous transport, thermal or optical characterization. Finally, there are several groups that push the MFM technique to the limits of high speed scanning, fast signal processing and recording than allow exploring high frequency processes.

Often the realistic experimental needs require measurements in a specific, precisely defined environment, e.g. temperature (i.e. low, high, or variable), pressure, humidity, specific gas atmosphere, vector magnetic field. Typically all these options are not available commercially but rather custom-developed as a research tool (See section 3a). Another rapidly filling niche is the development of custom-made magnetic probes. While commercial suppliers usually offer magnetic probes of three main types (i.e. standard, low-/high-moment), the customized options provide a significantly larger variety of probes with properties targeted to a specific (sometimes very narrow) application. The examples include the probes functionalized with magnetic nanoparticles and microsized beads, Fe-filled CNTs, one-side coated switchable probes, lithographically modified probes (e.g., figure 5), etc. Another important option is an ability to separate magnetic and electrostatic signals and successfully eliminate the latter. This is an imperative option for samples with low conductivity or electrically biased devices[118,119,145,228]. One of the most promising trends is development of new multifunctional systems, allowing combined mapping of magnetic and additional functional properties (e.g., KPFM-MFM, MF-PFM, MF-SEM, etc.), or measurements of magnetic properties by different means [e.g. in tandem MFM and magneto-optical Kerr effect microscopy (MFM-MOKE)]. All these combined modes are currently available only as custom-developed options (often due to a limited size of the specialized market). However, it might be expected that they will soon find their way to commercial options.

For the latter example, the combination of a MOKE microscope and MFM provides an interesting and powerful tool to study novel magnetic materials[229], not only at different length or time scales, dictated by the two methods, but also allows for flexibility in terms of the magnetic sample to be investigated in a highly efficient manner. For example, by utilizing the MOKE one can tune the domain pattern or magnetization state of the sample

and image within the, diffraction limited, resolution of the microscope. Then subsequent MFM investigations can follow which would allow for higher spatially resolved images to be taken. This combination has been utilized to image the domain structure of NbFeB crystals[230]. In this work two data analysis techniques were used to further gain insight to the magnetic structure, including surface charge pattern and local susceptibility. This is achieved by taking the difference and sum images, respectively, of two subsequent scans with oppositely magnetized probes. This allows the general domain structure through charge contrast images and also the variation in the sample permeability through the susceptibility contrast images to be obtained. Due to depth sensitivity of the two techniques complimentary information of the surface as well as the general magnetization structure within the domain can be investigated. Such functionality has significant merits for topics that are currently investigated and featured in this Perspectives section. For instance, systems hosting skyrmions or bubble domains could be studied using this combined approach. Due to the different skyrmion sizes possible, a cross-over between the two techniques would be defined: Kerr effect for a general overview and location of optically resolvable features and MFM, which would be used as more local probe to investigate the stray field signatures of the skyrmions. This particularly interesting in terms of the field protocol used to nucleate and annihilate skyrmions as it would allow for a broad understanding of the regions of most interest in a timely fashion rather than searching within the field-of-view of the SPM. Although the original combination of MFM and MOKE was published relatively long time ago[229], there is now a clear industrial interest from the companies in resuming this type of instrumentation on a commercial scale.

Multi-functional microscopes, with the ability to combine data from different sources into a single image as well as controllably and reproducibly modify the sample's state, are becoming more and more ubiquitous. For instance, quite recently, it has become possible to use an AFM inside of the SEM chamber to combine the two imaging techniques[231,232] or to perform nanofabrication with the focused-ion beam (FIB)[233].

The new instrument, called (AF-SEM), works in vacuum conditions and allows for large scanning areas and positioning the probe in ways that are typically non accessible to normal MFM. This is of interest when considering the possible shift from 2D fabrication towards 3D magnetic nanostructures, since AF-SEM will enable navigating complex samples and perform MFM on different faces of a 3D structure[205].

Another interesting system, in particular for in-liquid MFM[234], is a combination of SPM and optical microscope where the latter includes such functionalities as confocal- or fluorescence microscopy. The combination of MFM with these techniques will further enable a range of Life Science studies (e.g. related to MNPs applications or combined magnetic and optical labelling)[150]. For example, in a typical experiment where the cells are sensitive to light, proteins marked both with MNPs and fluorescent markers are introduced to the extracellular medium. Using either fluorescent or confocal microscopy, it is possible to study the large scale distribution and see if the MNPs are internalized by the cells, while using the MFM it is possible to detect individual MNPs and characterize their distribution at the nanoscale level inside of the cell without having to expose the cell to high intensity light[235,236].

Apart from combining different imaging techniques, the possibility of performing manipulation or modifications on the samples under study during imaging is a growing trend that has seen big developments in the last couple of years. For example, some SPM systems now include a lithography mode where the probe follows

a custom-defined path, while deflection or bias voltage are being applied to the probe[122,171,237]. Such experiments have been performed to move/capture magnetic beads, to induce defects/nucleation sites in magnetic films, and more recently, to print 3D nanostructures. The possibility of inducing defects/nucleation sites in magnetic films and nanostructures has a wide range of applications, since the lithography mode allows direct introduction of desirable magnetic sites, while MFM enables imaging the magnetization distribution and its consequent evolution. Additionally, the possibility to manipulate magnetic beads using MFM enables single magnetic bead studies. Finally, the 3D-printer AFM, which operates in-liquid and uses a hollow probe to deposit materials[238], is a system that has so far demonstrated rapid nanofabrication capabilities, without the need of a clean-room or e-beam lithography, which are expensive facilities that limit the access to nanofabrication. This is an excellent system to be combined with MFM, since the 3D printer enables building magnetic nanostructures, and the MFM allows imaging them to check if the magnetic nanostructure behaves as expected.

The ability to perform real-time MFM is a desired function for researchers in micro-/nano-magnetics as it would combine operational simplicity and availability of an SPM system in non-specialized environment with the power to map real (quasi-)dynamic effects, rather than "freeze-frames". Such advancements would allow for the study of effects such as domain wall propagation/creep or magnetization relaxation in MNPs with relative ease and high resolution. High-speed AFM (HS-AFM) is not a new concept, with commercial systems capable to map topography with sub-100 ms time-resolution rather than minutes in standard AFM[234], but speeds required to study a multitude of dynamic magnetic effects (potentially μs resolution and below) appears to be unlikely within the current scope of developments (as of time of writing) for MFM.

Another interesting concept in MFM-instrumentation is the ability to perform volumetric magnetic measurements. Until recently, SPM was traditionally performed in zero- (e.g. noise measurements), one- (e.g. variably-field MFM), or most typically two spatial dimensions in the sense that a change in physical interaction between the probe and the sample is quantified within a defined Cartesian coordinate above the basal plane of the surface. More advanced SPM techniques have extended into the third dimension by mapping chemical/physical properties with respect to: physical matter interactions (e.g. vibrational modes in chemical bonds by tip/surface-enhanced Raman[239] and scanning nano-IR microscopy[240]) or *xyz* (i.e. volumetric) data-acquisition (e.g. AFM force volume measurements[241,242]). Volumetric MFM can be performed on commercial instruments as it is largely based on the force volume methodology; the fast axis in such measurements is the z-axis, thus the probe generates force curves at each *xy*-pixel coordinate, mapping the phase change as a function of z-displacement (Fig. 9). Despite this, MFM has instead largely stayed within a single spatial plane, despite the recent scientific drive towards "big data" in other areas[243]. The likely causes for this shortfall thus far is large data-sizes and lengthy acquisition times.

3D-data for MFM does not exclusively refer to the three spatial dimensions, and there are many examples where the 3rd variable is an alternative controllable property such as temperature or applied field, which have been discussed throughout the Review section. A recent example of acquiring 3D matrices of MFM data is provided by demonstration of the general-mode (G-Mode) SPM system[243]. This system samples the entire photodetector response of an SPM with a MHz sampling rate, generating a three-dimensional datasets (after post-segmentation). One interesting application for G-Mode is the identification and separation of magnetic and electrostatic interactions in MFM[244].

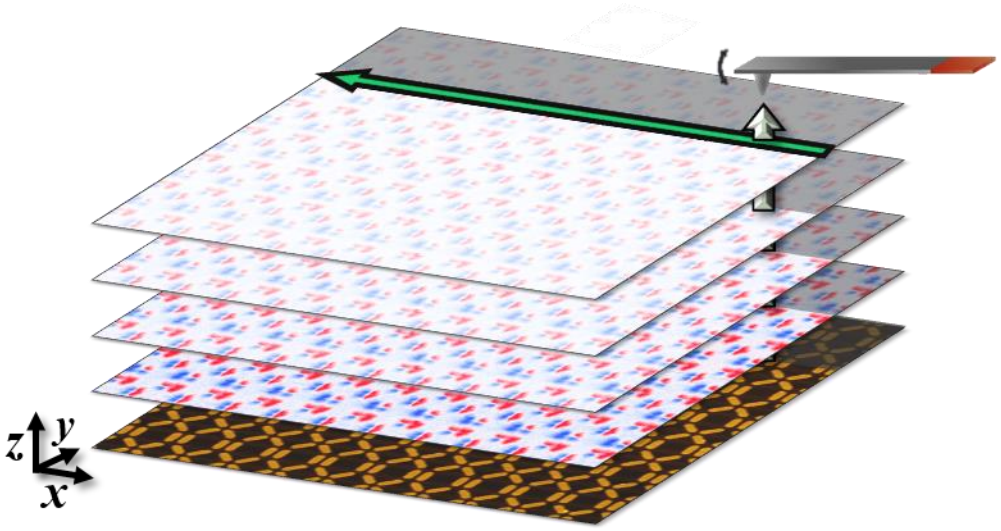

Figure 9: 3D-MFM. Schematic representation of volumetric MFM. The data is acquired by *z*-axis orientated force curves at each *xy*-coordinated pixel across the sample surface.

However, volumetric MFM datasets remain uncommon, despite improved data acquisition (in part developed from the popularity of functions such as force-volume), and more available tools/software for 3D-data visualization and analysis[245–247]. Volumetric MFM is largely an under-researched area which, with further development of data-handling practices, statistics, and with utilization of modern techniques such as machine learning, interesting properties could be quantified on the nanoscale without specialized/expensive equipment, e.g. 3D calibrated characterization of MNP's stray field, magnetization dynamics with respect to perturbing fields, or probe calibration/characterization.

The development of new MFM instrumentation goes hand-in-hand with the development of new magnetic probes built on demand (both custom-made and commercial). Customized probes are used to perform very specific tasks and push the limits of commercial MFM systems, e.g. to achieve a higher resolution; reduce/increase probe-sample interaction; or to be able to combine different scanning modes. An example of the latter is the use of a probe that is both magnetic and conductive simultaneously, enabling the instantaneous extraction of both magnetic and electrical signals[45].

Due to targeted specificity and high production costs, the market for customized probes is often small, thus many of the proposed modifications do not became available as commercial products. However, occasionally some of the new designs become commercially valid due to a reduction in fabrication costs and growth of the market for MFM (and other SPM techniques)[123]. The MFM probe with partial coating[248] is an example of this, where only one side of the probe's tip is coated with magnetic material; this reduces the magnetic moment of the probe, achieving a higher spatial sensitivity. The magnetic coating of this probe model is deposited in such a way to prevent also coating the cantilever with magnetic material, reducing the cantilever-sample interaction. Another example of custom probes entering the market is the MFM probe where the magnetic element is either inside or at the end of a CNT attached to the probe's apex. These probes are suitable for commercialization due to their apparent advantages (very low magnetic moment, high spatial resolution and extremely low probe-sample

interaction), which are becoming more and more critical in such growing fields such as bio-magnetism or magnetic topological structures (e.g. skyrmions).

An emerging technology is the multifunctional nanoscale sensor, which is able to detect several types of interaction simultaneously, rather than being used only for a single application. Examples of this include the use of magnetic probes in near-field systems such as scanning near-field microscopy[249], or tip-enhanced Raman spectroscopy[250]. This multifunctional approach would allow the production of probes to be more cost-effective. For example, the single application probe used in scanning thermal microscopy has very costly fabrication steps, but the addition of a magnetic coating, to create a multi-functional probe, would add only a relatively small cost to the total amount. In addition to the economic advantage, multifunctional probes are able to significantly reduce imaging time as they are able to simultaneously extract several different data types. It could be argued that the data quality would also be increased as the necessity to locate the area of interest with a multiple probes would be eliminated.

Despite the limitations faced in making customized probe models widely available, there are several examples of new probe models being adopted by MFM probe suppliers. While the probes with single functionality are expected to continue to dominate the MFM market in the short term, the multifunctional approach is expected to see greater success in the medium to long term, due to increased cost-effectiveness and added probe functionalities that advantage users.

b. CALIBRATED MFM

Typically macroscopic magnetic field measurements are traceable to nuclear magnetic resonance quantum standards and traceability chains to industry are already well established. However, these calibration chains only relate to measurements of fields that are constant and homogeneous over macroscopic volumes or surface areas down to the millimeter scale. At the same time, key international high-tech industries such as magnetic sensor manufacturing, precision position control and sensing in information technology, consumable electronics and Life Science as well as in R&D require traceable and reliable measurements of magnetic fields and flux densities on the micro- or nanometer scale, e.g. for quantitative analysis and quality control. In order to address the gap between the technological capabilities and the industrial needs, a collaborative European metrological project (NanoMag[1]) has been established. The overall goal of this project is to develop and provide coordinated and sustainable European metrology capabilities that extend reliable and traceable measurements of spatially resolved magnetic fields down to the micrometer and nanometer length scale. Development of the standards for traceable calibrations for MFM is one of the primarily goals of this project. The prime outcome of the project are related to development, comparison and validation of calibration procedures for traceable quantitative MFM measurements as well as establishing a high level of metrological MFM capabilities across Europe.

[1] http://www.ptb.de/empir/nanomag.html

Quantitative stray field measurements on the sub-50 nm length scale, which can be easily achieved by qMFM, have a multitude of applications. One of the largest is the realization of position control devices, which due to the much-reduced length scale will find use in appliances, automotive and consumer electronics. Furthermore, tailored magnetic stray field landscapes on the micrometer and nanometer length scale allow controllable magnetic micro- and/or nanoparticle manipulation and transport[220,251] in future cost-efficient lab-on-a-chip devices for biological, chemical, medical, and life science applications. Finally, a multitude of scientific studies, which are already tackled by MFM (see Section 3c) would benefit from a quantitative analysis. We just mention two large fields: (a) isolated nanoscopic object, which size and magnetic nature are not fully known (e.g. core-shell particles (see section 3b) with a non-magnetic oxide shell, structured thin film elements with a magnetically dead layer) and cannot satisfactorily be studied by global magnetometry, but could be quantified microscopically. (b) Reconstructing the magnetization state from stray field data is an ill-posed inversion problem in magnetostatics. This is even more problematic, when inhomogeneous magnetization structures or magnetization textures are to be resolved. While qMFM may not be able to unambiguously reconstruct such textures due to fundamental limitations, it allows to decide between different hypothetical models. Thus, inhomogeneous magnetization states, such as stripe domains in films with weak PMA (sections 3c) or skyrmions (section 4c) can be identified and distinguished from band domains or bubble domains when MFM measurements are analyzed quantitatively.

With increasing automation of both measurement capabilities and analysis procedures in modern AFM/MFM instrumentation, qMFM based on the most versatile TTF approach will become accessible for routine MFM experiments. The most important requirements are the availability of appropriate reference samples and of dedicated analysis software. Few groups do already have these capabilities[25,54] and they are currently being evaluated and developed further for dissemination to the public in the current European metrology project NanoMag[1], including analysis software tools in the scanning force data analysis package Gwyddion[245]. A second requirement is the availability of artefact-free, low noise and reproducible MFM data, which is aided by the improved stability and ease-of-operation in modern SPM-instrumentation.

Automation of measurement procedures (using scripting and batch processing) will allow repeated measurements with unchanged parameters (for improved signal-to noise), repeated measurements with systematically changing parameters (e.g. varying lift height for confirming the correct decay behavior of stray fields and thus excluding artefacts) and also alternating measurements between reference sample and the sample of interest (to judge the stability or wear of the probe's imaging properties during repeated use). Automation of analysis procedures will easily allow for e.g. drift corrections, averaging, or more complex mathematical operations (filtering, deconvolution, etc.) of images, which finally results in a quantitative evaluation of the MFM probe or the magnetic sample under study.

We further describe a required standard procedure for calibration. Prior to an automated quantitative measurement of a sample under study (i.e. measurand), MFM probe, reference sample and measurement procedure have to be properly selected to reveal the desired information. The main characteristic of a reference sample is such that its domain or stray field pattern can be quantitatively constructed from the measured MFM data without detailed knowledge of the yet to be calibrated probe. A reference sample can be a thin film with known PMA and saturation magnetization in a multi-domain state (see 3c), the stray field landscape of patterned

thin film elements in a single domain or the stray field of current-carrying wire structures. Most important for the choice of reference sample is that it covers all spatial frequencies present in the studied sample.

A standard procedure for quantitative MFM is envisioned as a flow diagram (Fig. 10). An alternative to the final block (red) is to develop a hypothetical surface charge/stray field model of the sample and construct a theoretical MFM pattern via convolution with the agreed TTF. The model should be modified until sufficient agreement with the experimental MFM pattern is achieved.

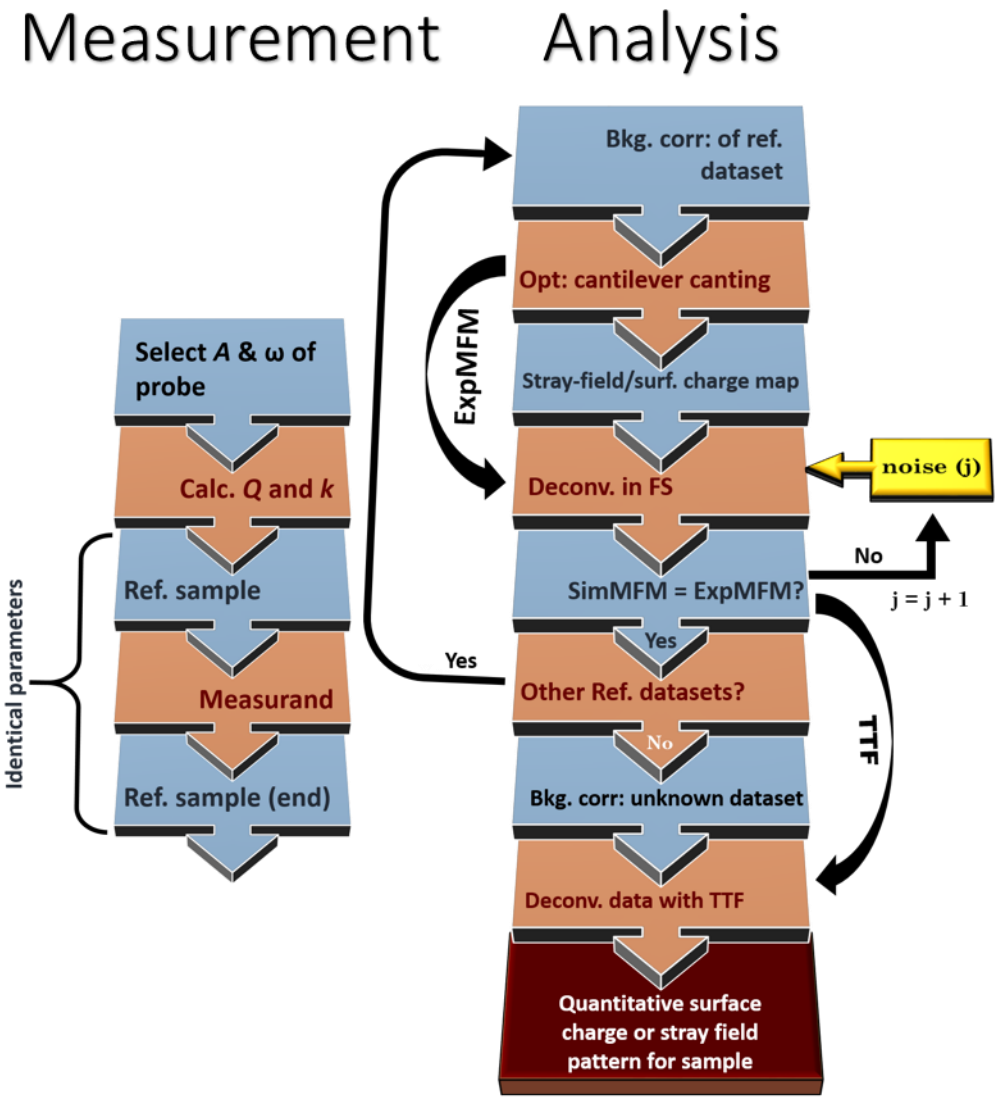

Figure 10: Flowchart for the calibrated MFM process. Flow diagram of the standard measurement (left) and analysis (right) procedure which should be adopted for calibrated/quantitative measurements by MFM.

c. NOVEL OBJECTS FOR MFM STUDIES

We further discuss application of MFM to studies of advanced and emerging magnetic materials and structures, namely antiferromagnets, spin-caloritronic materials, skyrmions, topological insulators, 2D materials

and van der Waals crystals as well as application of MFM to multidisciplinary life Science and environmental studies, which are often beyond a 'traditional' physics approach.

The applicability of MFM to characterize the stray magnetic fields from magnetic recording (MR) and logic devices is historically well established in literature. In earlier studies, Rugar *et al.*[32] reviewed the application of MFM to longitudinal recording media, and ever since there has been numerous studies of MR by MFM along with a host of other techniques. However, the bit capacity for modern MR (e.g., those based on perpendicular MR devices) has accelerated to the point where they are almost beyond the limits of the spatial resolution for standard MFM. As a consequence, MFM is currently a confirmatory technique for characterizing stray fields in MR devices industrially; used in tandem with other imaging methods. Further development in MR is certainly going to continue at pace, potentially circumventing the practicality for MFM imaging devices directly as it will not be able to fully resolve the structures. However, MFM's simplicity and availability means that, although it may not be used to characterize MR devices directly as has been done historically, it may remain a popular tool for research in this area in other ways, as we have seen for heat- or microwave-assisted magnetic recording (HAMR and MAMR, respectively[89,252,253]. These are modern technologies set for commercial markets. Examples of some creative studies into these devices by MFM includes work by Chen *et al*., who used MFM and MOKE to probe the erasure of the pre-recorded magnetic patterns as a function of laser power[254], and to experimentally study a novel bi-layered HAMR architecture that has one layer for conventional MR and a dedicated servomechanism in the underlayer[255]. More novel MR concepts, such as racetrack memory (see section 3c) shall remain a significant research topic as MFM offers the ability to image the domains in a quasi-dynamic state, and quality test the imperfections in NWs, which currently limit the DW velocities in devices.

Antiferromagnetic materials are interesting for spintronic applications due to the great variety of inherent phenomena they possess[256,257]. These include absence of stray fields due to fully compensated magnetic moments, resilience to externally applied fields and faster spin dynamics than those of FM materials due to high magnetic resonance frequencies of the order of THz. These properties make them attractive for applications such as antiferromagnetic-based memory. It has recently been demonstrated that current induced torques can be used to shift the orientation of the Néel vector in CuMnAs[258], resulting in the all electrical reading and writing of antiferromagnetic recording media. Indeed, thin films of Cr_2O_3 have been studied due to their ME effect which can be significantly enhanced when the thickness dimensions are of the order of a few nanometers[259]. Here, MeFM has been extremely successful in identifying the antiferromagnetic domains in Cr_2O_3. Furthermore, the antiferromagnetic properties of Cr_2O_3 combined with its ME effect can be used as an active exchange bias layer that can be modified electrically which can manipulate the FM state of exchange coupled magnetic layers[260].

It is expected that both MFM and MeFM will be adopted on a broader scale in order to understand better the local magnetic properties of antiferromagnetic materials. The intrinsic properties and hence the functionality of such materials are extremely dependent on the local degree of disorder and defects. The information gained by MFM and MeFM will be invaluable for the miniaturization of current antiferromagnetic based spintronic, multiferroic systems[261] and understanding of the role defects play in these materials. This is evident in recent investigations of multiferroic hexagonal rare earth manganite where MeFM was used to observe ME domains on a micrometer scale[95]. Here it was evidenced, by observing a divergence in the ME effect near the tri-critical point

using MeFM, that an enhancement of the ME effect in *h*-$ErMnO_3$ could be possible by utilizing critical fluctuations. Combinations of MeFM and MFM at low temperatures are anticipated to play a crucial role in the understanding and further development of multiferroic and antiferromagnetic materials exhibiting ME coupling on the micro and nanoscale.

Further to the investigation of antiferromagnetic order by MeFM[35,97], applications of MFM are likely to be employed for studies of defects in antiferromagnetic materials such as NiO. It has been shown that crystallographic defects can exhibit significantly different magnetic behavior to that of the lattice, where MFM was used to visualize dislocations at the individual level[262]. Moreover, it was found that it was possible to create such dislocations in order to generate high stability and high coercivity FM elements embedded in an antiferromagnetic environment, where the ferromagnetism arises due to the off-stoichiometry of the dislocations.

Here we discuss spin caloritronics, highlighting particularly interesting topics within the field, and discuss how MFM and other scanning probe techniques may elucidate to the underlying complex nature of the systems involved in this developing research topic. Spin caloritronics studies the combination of thermoelectric properties and spintronics, i.e. heat currents and spin currents[263]. This combination potentially offers benefits in efficiency over traditional Seebeck effect based devices, such as thermoelectric power generators[264,265] for energy harvesting applications[266]. A particularly interesting system that is highly studied in the field spin caloritronics is a thin film of heavy metal exhibiting spin-orbit interaction on top of a FM insulator[267]. Pt/YIG bilayers are popular candidates chosen to investigate phenomena such as spin pumping[268–271] where the FM YIG is used to drive a spin current into the Pt, which is detected via the inverse Spin Hall effect (ISHE), a manifestation of the spin-orbit interaction[194,272–276]. These systems are also used to observe the spin Seebeck effect (SSE)[267,277,278] where temperature gradients are used to generate a thermally induced spin voltage in the heavy metal layer, related to the magnetization dynamics of the magnet material in the thermal gradient. Again, the ISHE is used to as a spin current detector to measure the magnitude of the conversion. Of particular interest is the interface between the two layers where investigations have shown that magnetic proximity effects could exist, which have driven intense discussion[279–282]. Here, an induced moment in the nonmagnetic heavy metal layer could convolute the interpreted signal with additional effects such as the anomalous Nernst effect. Further to this, recent x-ray magnetic circular dichroism (XMCD) experiments have led to the debate[283] of the size of such an induced moment of Pt in Pt/YIG samples. Polarized neutron reflectivity (PNR) is an extremely sensitive technique which allows the layered magnetic structure of a material to be probed which has also revealed an induced magnetic moment at the Pt/YIG interface[284] in these types of bilayer samples.

Previously, there has been little in the way of local scale analysis/observation of the SSE in Pt/YIG type samples. Local laser heating experiments have been used to observe the effect with a resolution of approximately 5 μm in Hall bar type devices[285]. Therefore, it is highly expected that MFM and other relevant techniques (i.e. MFM + MOKE, or MFM + SThM) will be used to shed light on the complexity of this type of materials and reveal new insights. Here, high spatial resolution and sensitivity to the perpendicular field gradients could potentially elucidate the magnetic properties and domain structures close to the interface.

Skyrmions are chiral magnetic spin textures that are non-trivial and topologically stable[286,287]. Due to these characteristics they have been shown to demonstrate interesting phenomena such as the skyrmion Hall effect[173,288]

and the topological Hall effect[289–292] and therefore present an interesting platform for investigation of emergent electromagnetism associated with skyrmions. Fig. 11a-b shows example vector fields for Néel and Bloch skyrmions of certain chirality respectively, the color scales depicts the z-component of the spin and the insets show a cross-sectional dataset for each skyrmion highlighting the internal spin texture. Skyrmions are known to exist in bulk non-centrosymmetric chiral crystals[66,293–295] and also stabilized in highly engineered thin-films comprising of FM/heavy metal interfaces[296], which can host skyrmions above room temperature[297]. Due to the inherent or engineered inversion asymmetry found in these lattices or layered interfaces, a DMI is induced[291] which contributes to the overall magnetic ordering and tends to cant neighboring spins in favor of pure parallel/antiparallel Heisenberg exchange interaction, thus generating chiral spin structures. Due to their small size, theorized to range from 1 nm to 1 μm depending on the interplay of mechanisms that stabilize them[298] and ability to be generated and manipulated by SOT[76,297,299–301], it is expected that skyrmions will give rise to a range of new skyrmionic based logic and storage elements for future computer technologies, which scale beyond dimensions predicted by Moore's Law[287]. Among other imaging techniques[296], MFM has been used to image skyrmions and estimate the DMI value, as it allows a relatively wide field of view and high resolution to determine parameters such as the domain periodicity which can be used as an input parameter to numerically estimate the average DMI value[302].

Latest examples of qMFM have highlighted the possibility to attain a deeper understanding of the nanoscale magnetic complexity of skyrmions. Recent developments in implementing quantitative approaches have progressed the use of MFM in skyrmionic research from a simple imaging tool to an integral analysis procedure, which is the key to understanding vital aspects of the magnetic characteristics of skyrmions. Yagil *et al*. have demonstrated that MFM can be used to study the stray field profile of skyrmions in sputtered Ir/Fe/Co/Pt multilayers[75]. By employing a closed expression from a multipole expansion and a simulated stray field from the MFM probe, it was demonstrated that fitting the experimental data could reveal insights into the topological properties of the skyrmions. This approach allows for the determination of the skyrmion texture and distinguish between Bloch and Néel type skyrmions, demonstrating with reasonably certainty the prevailing nature of Néel-type skyrmions. Rather than using a simulated MFM probe as Yagil *et al.* [75] utilized an alternative approach that can be used to gain an insight into the magnetism on nanometer length scales. Baćani *et al*. have recently demonstrated through qMFM[130,142] that it is possible to quantify the variation in DMI in sputtered Ir/Co/Pt multilayers to nanoscale precision[302]. These observations elucidate the need of the significantly higher current densities required to initiate skyrmionic motion in multilayered systems (~ 10^{11}A.m^{-2})[297] compare to those in bulk materials (~ 10^{6}A.m^{-2})[298] . Here, the authors used the TTF method to calibrate the instruments response, which is required when pushing the limits of the measurement towards the resolution limit of the instrument. This takes into account the physical characteristics of the cantilever, magnetic properties of the MFM probe and also characteristics specific to the instrument such as the angle at which cantilever is mounted into the system. This method allowed observations of significant inhomogeneity in the DMI values of multilayers, revealing that variations up to 75% of the average value of the DMI can exist in spatial regions of ~50 nm. Thus, qMFM represents a considerable improvement in understanding of inhomogeneity at a nanoscale level of precision. The authors estimated that this corresponds to variations in the Co layer thickness equal to ±1.2 monolayers underlying the high level of control required to make skyrmion based memory and logic a reality.

It has recently been demonstrated that not only can MFM play a critical role in the determination of the properties of skyrmions but also MFM can be used to manipulate the magnetism in thin-films that exhibit DMI and generate skyrmions. Zhang *et al*. [303] showed that it is possible to use the stray magnetic field from an MFM probe to effectively slice the domain structure in a sample that had an initial starting point in the magnetostatic ground state and displayed a stripe-like domain pattern. By repeatedly scanning the surface it was possible to cut the stripe domains into skyrmions in the absence of an applied magnetic field and at room temperature. The TTF approach was used to calculate the stray field from the different types of probes used in the experiment to understand the magnitude of the *z*-component of the magnetic at the sample surface where the interaction occurs.

These examples capture the powerful way in which MFM can be extended by incorporating quantitative methods, such as the TTF approach, to extract information about a sample that is otherwise difficult to achieve. It is expected that as quantitative methods become wider spread a proliferation in these types of insightful experiments will shed light in emerging areas of magnetism at the nanoscale.

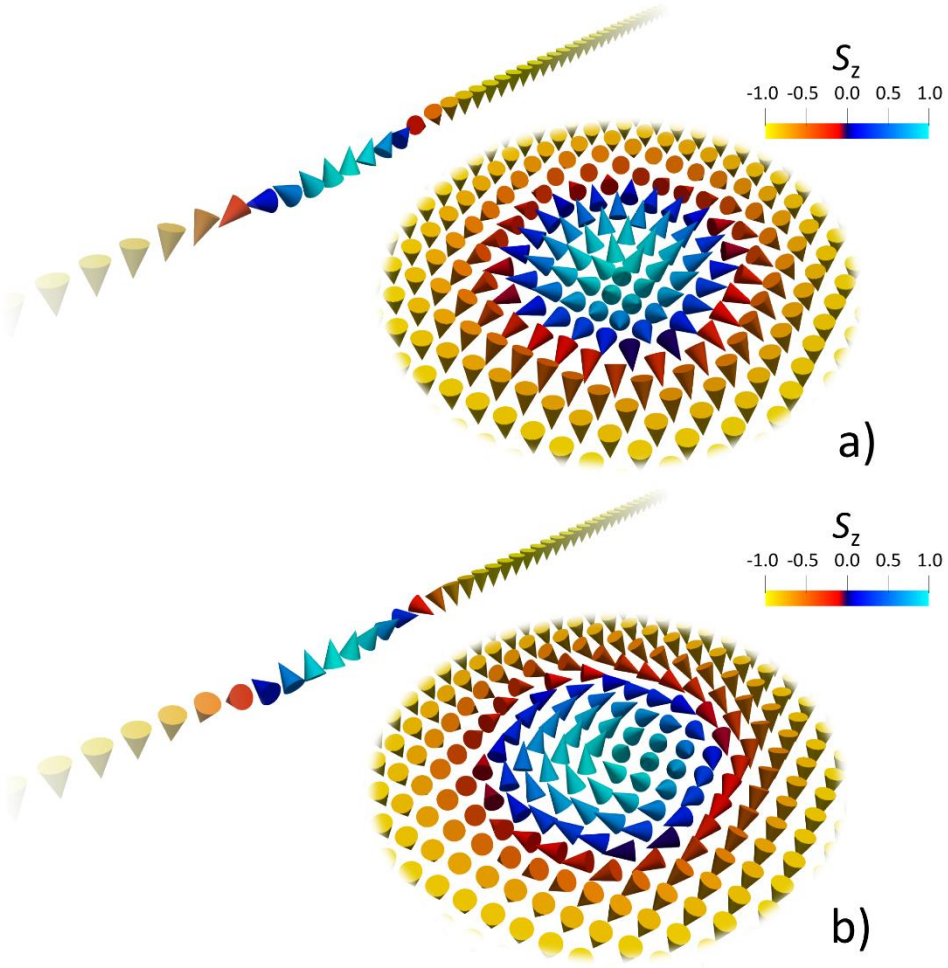

Figure 11: Skyrmions. Vector fields for; **a)** Néel and **b)** Bloch skyrmions occurring in multilayer systems exhibiting interfacial DMI and non-centrosymmetric crystals with bulk DMI, respectively. The insets (top left in each panel) display cross-sectional spin configurations through their skyrmion centers, highlighting the

differences in the spin reorientation of the Néel and Bloch skyrmion. The color bars represent the normal z-component of the magnetic moment within the skyrmion.

Topological Insulators (TIs) are unique electronic materials that, in addition to a bulk band gap similar to an ordinary insulator, have protected conducting states on the edge or surface that are possible due to the combination of spin-orbit interactions and time-reversal symmetry. Besides a huge fundamental interest, ferromagnetic TIs hold a great promise for applications in spintronics, metrology, and quantum computing. However, due to complexity of sample preparation and cryogenic temperature of operation, so far, relatively limited number of MFM studies have been reported for topological insulators. Wang *et al.*[304] have performed a systematic *in situ* cryogenic MFM study of FM domains in both single-crystal and thin-films samples of magnetic TIs, Cr-doped $(Bi_{0.1}Sb_{0.9})_2Te_3$. Bubble-like FM domains were observed in both single crystals and thin films. In the latter, smaller domain size (~500 nm) with narrower DWs (~150 – 300 nm) were detected due to vertical confinement effect, suggesting that thin films are more promising for visualization of chiral edge states[304]. In a work by Niu *et al.*[221], cryogenic MFM was used to study intrinsic ferromagnetism and quantum transport transition in individual Fe-doped Bi_2Se_3 topological insulator NWs. The NW showed spontaneous magnetization with a T_c of 40 K. The intrinsic ferromagnetism and gapped topological surface states in individual NWs suggest a pathway for future memory and ME applications. As the research interest in the field will only grow in near future, application of advanced MFM modes (i.e. in-field low temperature MFM as well as qMFM) is expected to accelerate to provide valuable information about these fascinating materials.

2D materials are another emerging class of modern artificial materials with exceptionally rich fundamental properties. Creating modern, smart materials with precise control over their physical properties is crucial for a wide range of applications and, as a trend, is most pronounced in the area of atomically thin 2D materials and their heterostructures. Such materials often possess unique and unexpected magnetic properties and MFM is a well-suited tool to validate and study them on nanoscale. For example, low-temperature in-field MFM was applied to studies of ferro-/antiferromagnetic transitions in a quasi-2D itinerant ferromagnet, Fe_3GeTe_2 [305]. In the local state, it was observed that the branching domain structure dynamically evolved into bubble domains as temperature decreased from 210 to 150 K, demonstrating existence of two distinct stable magnetic transitions and suggesting the existence of an instability in this temperature range.

In another recent study, the authors performed an MFM study of a new material system, which comprises of the InSe semiconductor van der Waals crystal and FM Fe-islands[306]. In contrast to many traditional semiconductors, the electronic properties of InSe are preserved after the incorporation of Fe. It was demonstrated that the formation of crystalline Fe-clusters in InSe induces a uniaxial internal magnetic field (~ 1 T) perpendicular to the InSe layers. Thus, this hybrid system, which consists of Fe-inclusions and a van der Waals crystal, enables the coexistence of magnetic and semiconducting properties within the same structure.

However, in a number of recent works on 2D materials MFM was used without applying the correct procedures and control tests, which led to rushed and not experimentally justified conclusions. For example, MFM was applied to characterize the mechanically and liquid exfoliated single- and few-layer MoS_2, graphene and graphene oxide nanosheets[307]. By analysis of the phase and amplitude shifts, the authors demonstrated that the magnetic response of MoS_2 and graphene is dependent on the layer thickness. It was shown that the mechanically and liquid

exfoliated single-layer MoS_2 demonstrated the reverse magnetic signal. At the same time, it was shown that graphene and MoS_2 flakes become nonmagnetic when they exceed a certain thickness. In this initial work, the authors performed merely a simple MFM study and the presence of electrostatic interaction was ruled out only on the basis of separate measurements on Fe_3O_4 and Au nanoparticles rather than directly excluded by the means of active Kelvin compensation. No experiments with probe magnetization reversal was performed and no clear explanation of the effect apart from a possible Li doping of MoS_2 was provided. In the follow up article by Lu Hua Li and Ying Chen[308], a more methodical and careful experimental study was performed. It was found that the MFM response had significant non-magnetic contributions due to capacitive and electrostatic interactions between the nanosheets of 2D materials and conductive cantilever tip, as demonstrated by EFM and SKPM analyses. In addition, the MFM signals of graphene and MoS_2 nanosheets were not responsive to reversed magnetic moment of the probe. Therefore, the observed MFM response was mainly originated from electrostatic artefacts and not compelling enough to imply intrinsic magnetism in graphene and MoS_2 nanosheets[308].

Similarly, MFM was used for studies of locally induced magnetization in strained $ReSe_2$ ribbons[309]. The authors observed a big negative phase shift on top of a folded ribbon, which they attributed to strong attractive interaction between the $ReSe_2$ wrinkles and the MFM probe. However, in this case as well the conclusions were drawn without a convincing control experiment (i.e. reverse of the probe magnetization, use of non-magnetic metal coated probe, etc.). Similarly to what was discussed earlier, the field of 2D materials in magnetism is extremely fast and successfully growing. While magnetic properties of such materials were somewhat late to be explored (primarily due to difficulty in synthesis of ferromagnets in 2D state), very recent development have demonstrated that this can be successfully overcome, opening the way for advanced MFM studies. As in the case of TI, it can be expected that such varieties of MFM modes as in-field and low temperature MFM as well as qMFM are to be applied.

Using HS-AFM both the structure and dynamic processes of biomolecules can be observed without disturbing their function[310]. The possibility to combine this technique with MFM would open new opportunities of characterization and manipulation of biological systems. Also the combination of AFM and inverted optical microscopy techniques, in particular Total Internal Reflection Fluorescence (TIRF) microscopy allows for simultaneous manipulation and imaging of samples, which can be applied for the measurement of mechanical properties of single proteins and the identification of specific components in complex assemblies[311]. For that reason, the combination of MFM, capable of e.g. detection of magnetic labels, and these optical techniques opens the possibility of nanomanipulation and simultaneous detection of different properties giving the chance to obtain information inaccessible with other techniques.

We further discuss the potential to use MFM in less traditional areas such as Life Science and environmental studies. In the case of *in vivo* applications, MNPs [i.e. superparamagnetic iron oxides (SPIOs)] integrated into the material of the mesh can be used, e.g., for the development of a surgical mesh implant that is visible in magnetic resonance imaging. In order to get a high quality mesh, a narrow size distribution and homogenous spatial distribution, as well as a strong magnetization of SPIOs within the filament of the mesh are required. Slabu *et al.*[312] used MFM to determine the beneficial properties for the assembly and imaging of the implant. These analyses showed the feasibility of visualization of surgical implants with incorporated SPIOs and the influence of

the agglomeration of SPIOs on their magnetization and on a homogenous spatial distribution within the polymer of the mesh. The findings demonstrate that MFM is a very promising tool for characterization of surgical implants.

In addition to the traditional use of magnetic materials in high-tech, advanced manufacturing, sensor and biomedical industries, they are also applied in geoscience, including climate change, pollution evolution, iron biomineralization and diagenetic processes in sediments[313]. Recently, the use of magnetic micro- and nanoparticles has been proposed as a crucial factor for water remediation[314] and oil recovery[315]. MFM (together with other characterization techniques) have been applied for a survey of different Fe-containing magnetic compounds targeting their use in environmental applications, such as in wastewater treatments and remediation, and revealing their advantages and drawbacks[316]. Due to its high resolution and sensitivity, capability to study rough surfaces (i.e. topographic and magnetic signals separation), possibility to detect simultaneously different interactions and properties, and to operate under different ambience conditions and magnetic fields, the MFM is a useful technique to perform magnetic analyse of environmentally relevant systems.

5. CONCLUSION

In the Review of the current state of the art we addressed the recent major developments in the field of MFM, including variety of the operational modes and new trends in instrumentation, such as in-field and variable field MFM, MFM under controllable temperature, electrostatic compensation, energy dissipation and MeFM. A variety of specialized, custom-designed magnetic probes (one-side and multilayer coated, functionalized with a MNPs, NWs of CNT filled with magnetic materials, etc.) were presented. Special attention was paid to commonly occurring artefacts in the MFM images and the way to deal with them. Modern objects of recent MFM studies were summarized, including objects such as thin films with PMA, multiferroic materials, and magnetic topological structures.

In the Perspectives we addressed the emerging MFM trends, concerning further development of instrumentation (e.g. in combination with other SPM modes and radiation techniques) and software, routes towards calibrated MFM imaging using either modeling approaches or physical means of and application of MFM to studies of advanced and emerging materials.

While commercial, off-the-shelf MFM systems still remain a valid indispensable tool for a routine inspection of magnetic properties of samples, modern challenges in both research and industry demand development of new advanced MFM modes. To fulfil this need, the current research is targeted in different directions including: development of a new MFM instrumentation and flexible software; novel types of MFM probes (a key point still under development); development of multifunctional MFM, through combination with other techniques; and targeting complex material properties, which is a general trend to make MFM compatible with simultaneous transport, thermal or optical characterization.

Another coming trend is the possibility to obtain volumetric MFM datasets (where the third dimension should be understood in a broad sense, e.g. probe-sample separation, magnetic or electrical field, etc.). This trend is well supported by advances in Big Data acquisition and handling (in part related to the popularity of force-volume functions) and availability of tools/software for 3D-data visualization and analysis. Further development of

volumetric MFM (and other SPM modes) is very closely aligned with development of data-handling practices, statistics, and utilization of machine learning and artificial intelligence. Following this trend, interesting properties could be quantified on the nanoscale without specialized/expensive equipment, e.g. 3D calibrated characterization of a stray field emanating from a nano-object, magnetization dynamics with respect to perturbing fields, or probe calibration/characterization.

Calibrated MFM will remain an important topic for development. While typically macroscopic magnetic field measurements are traceable to nuclear magnetic resonance down to the millimeter scale, here we outlined the need of such metrological procedures in respect to nanoscale characterization as well as development of capabilities that extend reliable and traceable measurements of spatially resolved magnetic fields down to the micrometer and nanometer scale. We also described a standard procedure for MFM calibration, which represents a comprehensive approach combining the experimental measurements of the reference and measurand samples with the analytical procedure involving image deconvolution in Fourier space using appropriate noise filters (e.g. Wiener Invert Filter) to reconstruct the tip transfer function. We believe that with increasing automation of both measurement capabilities and analysis procedures in modern AFM/MFM instrumentation, qMFM based on the most versatile TTF approach will soon become accessible for routine MFM experiments. The most important requirements along this route are the availability of appropriate reference samples and of dedicated analysis software.

We further discussed application of MFM to studies of advanced and emerging magnetic materials and structures (often extremely demanding in terms of resolution, sensitivity and physical environment), namely: antiferromagnets, spin-caloritronic materials, skyrmions, topological insulators, 2D materials and van der Waals crystals as well as application of MFM to multidisciplinary Life Science and environmental studies, which are often beyond a 'traditional' physics approach.

All these examples demonstrate why MFM remains a powerful characterization tool. Equipped with novel modes and additional functionalities, customized MFM is exceptionally well-positioned to become an even more indispensable technique, to be widely used in insightful experiments that will shed light in emerging areas of magnetism at the nanoscale.

6. Acknowledgements

Dr. R. Schäfer and Prof. R. Cowburn are thanked for their useful insights into the perspectives of the MFM+MOKE multifunctional technique; R. Nevill is acknowledged for assistance in the production of Figures 1 and 4; and S. Gorno and K. Edmonds are thanked for their assistance in reference management and general suggestions. OK, RP, CB, HC and VN acknowledge the financial support from the European Metrology Programme for Innovation and Research (grant number 15SIB06), NanoMag. M.J. and A.A. acknowledge the support from the Spanish Ministerio de Economia y Competitividad (MINECO) under projects MAT2015-73775-JIN and MAT2016-76824-C3-1-R.

7. REFERENCES

[1] Y. Martin and H.K. Wickramasinghe, Appl. Phys. Lett. **50**, 1455 (1987).

[2] J.J. Sáenz, N. García, P. Grütter, E. Meyer, H. Heinzelmann, R. Wiesendanger, L. Rosenthaler, H.R. Hidber, and H. -J. Güntherodt, J. Appl. Phys. **62**, 4293 (1987).

[3] D.A. Allwood, G. Xiong, M.D. Cooke, and R.P. Cowburn, J. Phys. D. Appl. Phys. **36**, 2175 (2003).

[4] A.L. Yeats, P.J. Mintun, Y. Pan, A. Richardella, B.B. Buckley, N. Samarth, and D.D. Awschalom, Proc. Natl. Acad. Sci. **114**, 10379 (2017).

[5] J.N. Chapman, J. Phys. D Appl. Phys. **17**, 623 (1984).

[6] H.P. Oepen and J. Kirschner, Scanning Microsc **5**, 1 (1991).

[7] E.C. Corredor, S. Kuhrau, F. Kloodt-Twesten, R. Frömter, and H.P. Oepen, Phys. Rev. B **96**, 060410 (2017).

[8] G. Schönhense, J. Phys. Condens. Matter **11**, 9517 (1999).

[9] X.M. Cheng and D.J. Keavney, Reports Prog. Phys. **75**, 026501 (2012).

[10] C.M. Schneider, J. Magn. Magn. Mater. **156**, 94 (1996).

[11] G. Balasubramanian, I.Y. Chan, R. Kolesov, M. Al-Hmoud, J. Tisler, C. Shin, C. Kim, A. Wojcik, P.R. Hemmer, A. Krueger, T. Hanke, A. Leitenstorfer, R. Bratschitsch, F. Jelezko, and J. Wrachtrup, Nature **455**, 648 (2008).

[12] L. Rondin, J.-P. Tetienne, T. Hingant, J.-F. Roch, P. Maletinsky, and V. Jacques, Reports Prog. Phys. **77**, 056503 (2014).

[13] H.J. Mamin, M. Poggio, C.L. Degen, and D. Rugar, Nat. Nanotechnol. **2**, 301 (2007).

[14] D. Rugar, C.S. Yannoni, and J.A. Sidles, Nature **360**, 563 (1992).

[15] A. Oral, J. Vac. Sci. Technol. B Microelectron. Nanom. Struct. **14**, 1202 (1996).

[16] J.R. Kirtley and J.P. Wikswo, Annu. Rev. Mater. Sci. **29**, 117 (1999).

[17] J.R. Kirtley, Reports Prog. Phys. **73**, 126501 (2010).

[18] E.O. Lachman, A.F. Young, A. Richardella, J. Cuppens, H.R. Naren, Y. Anahory, A.Y. Meltzer, A. Kandala, S. Kempinger, Y. Myasoedov, M.E. Huber, N. Samarth, and E. Zeldov, Sci. Adv. **1**, e1500740 (2015).

[19] L. Belliard, A. Thiaville, S. Lemerle, A. Lagrange, J. Ferré, and J. Miltat, J. Appl. Phys. **81**, 3849 (1997).

[20] M.R. Freeman and B.C. Choi, Science (80-.). **294**, 1484 (2001).

[21] A. Schwarz and R. Wiesendanger, Nano Today **3**, 28 (2008).

[22] Y. Seo, P. Cadden-Zimansky, and V. Chandrasekhar, Appl. Phys. Lett. **87**, 103103 (2005).

[23] A. Asenjo, M. Jaafar, D. Navas, and M. Vázquez, J. Appl. Phys. **100**, 023909 (2006).

[24] P. Ares, M. Jaafar, A. Gil, J. Gómez-Herrero, A. Asenjo, J. Gõmez-Herrero, and A. Asenjo, Small **11**, 4731 (2015).

[25] H.J. Hug, B. Stiefel, P.J.A. van Schendel, A. Moser, R. Hofer, S. Martin, H.-J. Güntherodt, S. Porthun, L. Abelmann, J.C. Lodder, G. Bochi, and R.C. O'Handley, J. Appl. Phys. **83**, 5609 (1998).

[26] U. Hartmann, Annu. Rev. Mater. Sci. **29**, 53 (1999).

[27] R. García and R. Pérez, Surf. Sci. Rep. **47**, 197 (2002).

[28] S.N. Magonov, V. Elings, and M.-H. Whangbo, Surf. Sci. **375**, L385 (1997).

[29] M. Whangbo, G. Bar, and R. Brandsch, Surf. Sci. **411**, L794 (1998).

[30] S. Vock, Resolving Local Magnetization Structures by Quantitative Magnetic Force Microscopy, Technischen Universitat Dresden, Germany, 2014.

[31] X. Zhao, J. Schwenk, A.O. Mandru, M. Penedo, M. Baćani, M.A. Marioni, and H.J. Hug, New J. Phys. **20**, 013018 (2018).

[32] D. Rugar, H.J. Mamin, P. Guethner, S.E. Lambert, J.E. Stern, I. McFadyen, and T. Yogi, J. Appl. Phys. **68**, 1169 (1990).

[33] T.R. Albrecht, P. Grütter, D. Horne, and D. Rugar, J. Appl. Phys. **69**, 668 (1991).

[34] C. Canale, B. Torre, D. Ricci, and P.C. Braga, in *At. Force Microsc. Biomed. Res. Methods Protoc.*, edited by P.C. Braga and D. Ricci (Humana Press, Totowa, NJ, 2011), pp. 31–43.

[35] F. Bi, M. Huang, S. Ryu, H. Lee, C.-W. Bark, C.-B. Eom, P. Irvin, and J. Levy, Nat. Commun. **5**, 5019 (2014).

[36] R. Puttock, H. Corte-Leon, V. Neu, D. Cox, A. Manzin, V. Antonov, P. Vavassori, and O. Kazakova, IEEE Trans. Magn. **53**, 1 (2017).

[37] J. Červenka, M.I. Katsnelson, and C.F.J. Flipse, Nat. Phys. **5**, 840 (2009).

[38] D. Martínez-Martín, M. Jaafar, R. Pérez, J. Gómez-Herrero, and A. Asenjo, Phys. Rev. Lett. **105**, 257203 (2010).

[39] T.L. Makarova, B. Sundqvist, R. Höhne, P. Esquinazi, Y. Kopelevich, P. Scharff, V. Davydov, L.S. Kashevarova, and A. V. Rakhmanina, Nature **413**, 716 (2001).

[40] D. Spemann, K.H. Han, R. Höhne, T. Makarova, P. Esquinazi, and T. Butz, Nucl. Instruments Methods Phys. Res. Sect. B Beam Interact. with Mater. Atoms **210**, 531 (2003).

[41] A. Talyzin, A. Dzwilewski, L. Dubrovinsky, A. Setzer, and P. Esquinazi, Eur. Phys. J. B **55**, 57 (2007).

[42] D.W. Boukhvalov, P.F. Karimov, E.Z. Kurmaev, T. Hamilton, A. Moewes, L.D. Finkelstein, M.I. Katsnelson, V.A. Davydov, A. V Rakhmanina, T.L. Makarova, Y. Kopelevich, S. Chiuzbăian, and M. Neumann, Phys. Rev. B **69**, 115425 (2004).

[43] T.L. Makarova, B. Sundqvist, R. Höhne, P. Esquinazi, Y. Kopelevich, P. Scharff, V. Davydov, L.S. Kashevarova, and A. V Rakhmanina, Nature **440**, 707 (2006).

[44] L. Angeloni, D. Passeri, M. Reggente, D. Mantovani, and M. Rossi, Sci. Rep. **6**, 1 (2016).

[45] M. Jaafar, O. Iglesias-Freire, L. Serrano-Ramón, M.R. Ibarra, J.M. de Teresa, and A. Asenjo, Beilstein J. Nanotechnol. **2**, 552 (2011).

[46] V. Panchal, R. Pearce, R. Yakimova, A. Tzalenchuk, and O. Kazakova, Sci. Rep. **3**, 2597 (2013).

[47] V. Cambel, D. Gregušová, P. Eliáš, J. Fedor, I. Kostič, J. Maňka, and P. Ballo, J. Electr. Eng. **62**, 37 (2011).

[48] A. Yacoot and L. Koenders, J. Phys. D. Appl. Phys. **41**, 103001 (2008).

[49] P.J. Grace, M. Venkatesan, J. Alaria, J.M.D. Coey, G. Kopnov, and R. Naaman, Adv. Mater. **21**, 71 (2009).

[50] M.A. Garcia, E. Fernandez Pinel, J. de la Venta, A. Quesada, V. Bouzas, J.F. Fernández, J.J. Romero, M.S. Martín González, and J.L. Costa-Krämer, J. Appl. Phys. **105**, 013925 (2009).

[51] J. Scott, S. McVitie, R.P. Ferrier, and A. Gallagher, J. Phys. D. Appl. Phys. **34**, 1326 (2001).

[52] S. Vock, Z. Sasvari, C. Bran, F. Rhein, U. Wolff, N.S. Kiselev, A.N. Bogdanov, L. Schultz, O. Hellwig, and V. Neu, IEEE Trans. Magn. **47**, 2352 (2011).

[53] F.M. Candocia, E.B. Svedberg, D. Litvinov, and S. Khizroev, Nanotechnology **15**, S575 (2004).

[54] S. Vock, C. Hengst, M. Wolf, K. Tschulik, M. Uhlemann, Z. Sasvári, D. Makarov, O.G. Schmidt, L. Schultz, and V. Neu, Appl. Phys. Lett. **105**, 172409 (2014).

[55] R.D. Gomez, in *Exp. Methods Phys. Sci.* (2001), pp. 69–109.

[56] T. Kebe and A. Carl, J. Appl. Phys. **95**, 775 (2004).

[57] J. Lohau, S. Kirsch, A. Carl, G. Dumpich, and E.F. Wassermann, J. Appl. Phys. **86**, 3410 (1999).

[58] M. Löhndorf, A. Wadas, G. Lütjering, D. Weiss, and R. Wiesendanger, Zeitschrift Für Phys. B Condens. Matter **101**, 1 (1996).

[59] A. Asenjo, D. García, J. García, C. Prados, and M. Vázquez, Phys. Rev. B **62**, 6538 (2000).

[60] C. Bran, A.B. Butenko, N.S. Kiselev, U. Wolff, L. Schultz, O. Hellwig, U.K. Rößler, A.N. Bogdanov, and V. Neu, Phys. Rev. B - Condens. Matter Mater. Phys. **79**, 1 (2009).

[61] R. O'Barr and S. Schultz, J. Appl. Phys. **81**, 5458 (1997).

[62] J.. García, A. Thiaville, and J. Miltat, J. Magn. Magn. Mater. **249**, 163 (2002).

[63] J. Bai, H. Takahoshi, H. Ito, H. Saito, and S. Ishio, J. Appl. Phys. **96**, 1133 (2004).

[64] M. Jaafar, R. Sanz, J. McCord, J. Jensen, R. Schäfer, M. Vázquez, and A. Asenjo, Phys. Rev. B - Condens. Matter Mater. Phys. **83**, 1 (2011).

[65] P. Kappenberger, S. Martin, Y. Pellmont, H.J. Hug, J.B. Kortright, O. Hellwig, and E.E. Fullerton, Phys. Rev. Lett. **91**, 267202 (2003).

[66] P. Milde, D. Kohler, J. Seidel, L.M. Eng, A. Bauer, A. Chacon, J. Kindervater, S. Muhlbauer, C. Pfleiderer, S. Buhrandt, C. Schutte, and A. Rosch, Science (80-.). **340**, 1076 (2013).

[67] E. Pinilla-Cienfuegos, S. Mañas-Valero, A. Forment-Aliaga, and E. Coronado, ACS Nano **10**, 1764 (2016).

[68] M. Jaafar, L. Serrano-Ramón, O. Iglesias-Freire, A. Fernández-Pacheco, M.R. Ibarra, J.M. de Teresa, and A. Asenjo, Nanoscale Res. Lett. **6**, 1 (2011).

[69] J.M. García, A. Thiaville, J. Miltat, K.J. Kirk, and J.N. Chapman, J. Magn. Magn. Mater. **242**–**245**, 1267 (2002).

[70] O. Ermolaeva, N. Gusev, E. Skorohodov, Y. Petrov, M. Sapozhnikov, and V. Mironov, Materials (Basel). **10**, 1034 (2017).

[71] T. Hauet, L. Piraux, S.K. Srivastava, V.A. Antohe, D. Lacour, M. Hehn, F. Montaigne, J. Schwenk, M.A. Marioni, H.J. Hug, O. Hovorka, A. Berger, S. Mangin, and F. Abreu Araujo, Phys. Rev. B - Condens. Matter Mater. Phys. **89**, 1 (2014).

[72] E. Berganza, C. Bran, M. Jaafar, M. Vázquez, and A. Asenjo, Sci. Rep. **6**, 29702 (2016).

[73] H. Mohammed, H. Corte-León, Y.P. Ivanov, J.A. Moreno, O. Kazakova, and J. Kosel, IEEE Trans. Magn. **53**,

1 (2017).

[74] R. Streubel, P. Fischer, F. Kronast, V.P. Kravchuk, D.D. Sheka, Y. Gaididei, O.G. Schmidt, and D. Makarov, J. Phys. D. Appl. Phys. **49**, (2016).

[75] A. Yagil, A. Almoalem, A. Soumyanarayanan, A.K.C. Tan, M. Raju, C. Panagopoulos, and O.M. Auslaender, Appl. Phys. Lett. **112**, 192403 (2018).

[76] A. Hrabec, J. Sampaio, M. Belmeguenai, I. Gross, R. Weil, S.M. Chérif, A. Stashkevich, V. Jacques, A. Thiaville, and S. Rohart, Nat. Commun. **8**, 1 (2017).

[77] V. Karakas, A. Gokce, A.T. Habiboglu, S. Arpaci, K. Ozbozduman, I. Cinar, C. Yanik, R. Tomasello, S. Tacchi, G. Siracusano, M. Carpentieri, G. Finocchio, T. Hauet, and O. Ozatay, Sci. Rep. **8**, 7180 (2018).

[78] D. Maccariello, W. Legrand, N. Reyren, K. Garcia, K. Bouzehouane, S. Collin, V. Cros, and A. Fert, Nat. Nanotechnol. **056022**, 1 (2018).

[79] C. Moya, Ó. Iglesias-Freire, N. Pérez, X. Batlle, A. Labarta, and A. Asenjo, Nanoscale **7**, 8110 (2015).

[80] C. Moya, Ó. Iglesias-Freire, X. Batlle, A. Labarta, and A. Asenjo, Nanoscale **7**, 17764 (2015).

[81] E. Nazaretski, K.S. Graham, J.D. Thompson, J.A. Wright, D. V. Pelekhov, P.C. Hammel, and R. Movshovich, Rev. Sci. Instrum. **80**, 083704 (2009).

[82] C.-H. Sow, K. Harada, A. Tonomura, G. Crabtree, and D.G. Grier, Phys. Rev. Lett. **80**, 2693 (1998).

[83] S. Eley, M. Miura, B. Maiorov, and L. Civale, Nat. Mater. **16**, 409 (2017).

[84] H.J. Hug, A. Moser, T. Jung, O. Fritz, A. Wadas, I. Parashikov, and H. -J. Güntherodt, Rev. Sci. Instrum. **64**, 2920 (1993).

[85] H.J. Hug, A. Moser, I. Parashikov, B. Stiefel, O. Fritz, H.-J. Güntherodt, and H. Thomas, Phys. C Supercond. **235**–**240**, 2695 (1994).

[86] G.C. Ratcliff, D.A. Erie, and R. Superfine, Appl. Phys. Lett. **72**, 1911 (1998).

[87] D. Ramos, J. Tamayo, J. Mertens, and M. Calleja, J. Appl. Phys. **99**, 124904 (2006).

[88] Ü. Çelik, Ö. Karcı, Y. Uysallı, H.Ö. Özer, and A. Oral, Rev. Sci. Instrum. **88**, (2017).

[89] D. Weller, G. Parker, O. Mosendz, A. Lyberatos, D. Mitin, N.Y. Safonova, and M. Albrecht, J. Vac. Sci. Technol. B, Nanotechnol. Microelectron. Mater. Process. Meas. Phenom. **34**, 060801 (2016).

[90] L.H. Lewis, C.H. Marrows, and S. Langridge, J. Phys. D. Appl. Phys. **49**, 323002 (2016).

[91] Y. Lee, Z.Q. Liu, J.T. Heron, J.D. Clarkson, J. Hong, C. Ko, M.D. Biegalski, U. Aschauer, S.L. Hsu, M.E. Nowakowski, J. Wu, H.M. Christen, S. Salahuddin, J.B. Bokor, N.A. Spaldin, D.G. Schlom, and R. Ramesh, Nat. Commun. **6**, 5959 (2015).

[92] S. Kim, D. Seol, X. Lu, M. Alexe, and Y. Kim, Sci. Rep. **7**, 1 (2017).

[93] L. Angeloni, D. Passeri, S. Corsetti, D. Peddis, D. Mantovani, and M. Rossi, Nanoscale **9**, 18000 (2017).

[94] M.P. Arenas, E.M. Lanzoni, C.J. Pacheco, C.A.R. Costa, C.B. Eckstein, L.H. de Almeida, J.M.A. Rebello, C.F. Deneke, and G.R. Pereira, J. Magn. Magn. Mater. **446**, 239 (2018).

[95] Y. Geng, H. Das, A.L. Wysocki, X. Wang, S.-W. Cheong, M. Mostovoy, C.J. Fennie, and W. Wu, Nat. Mater. **13**, 163 (2013).

[96] Y. Geng and W. Wu, Rev. Sci. Instrum. **85**, 053901 (2014).

[97] P. Schoenherr, L. Giraldo, M. Lilienblum, M. Trassin, D. Meier, and M. Fiebig, Materials (Basel). **10**, 1051 (2017).

[98] W. Wang, J.A. Mundy, C.M. Brooks, J.A. Moyer, M.E. Holtz, D.A. Muller, D.G. Schlom, and W. Wu, Phys. Rev. B **95**, 134443 (2017).

[99] R. Garcia and E.T. Herruzo, Nat. Nanotechnol. **7**, 217 (2012).

[100] J.W. Li, J.P. Cleveland, and R. Proksch, Appl. Phys. Lett. **94**, 2007 (2009).

[101] C. Dietz, E.T. Herruzo, J.R. Lozano, and R. Garcia, Nanotechnology **22**, 125708 (2011).

[102] J. Schwenk, M. Marioni, S. Romer, N.R. Joshi, and H.J. Hug, Appl. Phys. Lett. **104**, 1 (2014).

[103] A. Kaidatzis and J.M. García-Martín, Nanotechnology **24**, 165704 (2013).

[104] J. Schwenk, X. Zhao, M. Bacani, M.A. Marioni, S. Romer, and H.J. Hug, Appl. Phys. Lett. **107**, (2015).

[105] D. Liu, K. Mo, X. Ding, L. Zhao, G. Lin, Y. Zhang, and D. Chen, Appl. Phys. Lett. **107**, 103110 (2015).

[106] R. García, R. Magerle, and R. Perez, Nat. Mater. **6**, 405 (2007).

[107] P. Grütter, Y. Liu, P. LeBlanc, and U. Dürig, Appl. Phys. Lett. **71**, 279 (1997).

[108] A. Labuda, Y. Miyahara, L. Cockins, and P.H. Grütter, Phys. Rev. B **84**, 125433 (2011).

[109] Ó. Iglesias-Freire, J.R. Bates, Y. Miyahara, A. Asenjo, and P.H. Grütter, Appl. Phys. Lett. **102**, 022417 (2013).

[110] M. Jaafar, Ó. Iglesias-Freire, P. García-Mochales, J.J. Sáenz, and A. Asenjo, Nanoscale **8**, 16989 (2016).

[111] B. Torre, G. Bertoni, D. Fragouli, A. Falqui, M. Salerno, A. Diaspro, R. Cingolani, and A. Athanassiou, Sci. Rep. **1**, 202 (2011).

[112] M. Jaafar, D. Martínez-Martín, M. Cuenca, J. Melcher, A. Raman, and J. Gómez-Herrero, Beilstein J. Nanotechnol. **3**, 336 (2012).

[113] A. Schultz, D. Louder, M. Hansen, C. DeVries, and J. Nathe, IEEE Trans. Magn. **35**, 2571 (1999).

[114] M. Abe and Y. Tanaka, IEEE Trans. Magn. **40**, 1708 (2004).

[115] H. Corte-León, P. Krzysteczko, F. Marchi, J.-F. Motte, A. Manzin, H.W. Schumacher, V. Antonov, and O. Kazakova, AIP Adv. **6**, 056502 (2016).

[116] H. Corte-León, B. Gribkov, P. Krzysteczko, F. Marchi, J.-F. Motte, H.W. Schumacher, V. Antonov, and O. Kazakova, J. Magn. Magn. Mater. **400**, 225 (2016).

[117] V. Nabaei, R.K. Rajkumar, A. Manzin, O. Kazakova, and A. Tzalenchuk, J. Appl. Phys. **113**, 064504 (2013).

[118] R.K. Rajkumar, A. Asenjo, V. Panchal, A. Manzin, Ó. Iglesias-Freire, and O. Kazakova, J. Appl. Phys. **115**, 172606 (2014).

[119] V. Panchal, H. Corte-León, B. Gribkov, L.A. Rodriguez, E. Snoeck, A. Manzin, E. Simonetto, S. Vock, V. Neu, and O. Kazakova, Sci. Rep. **7**, 7224 (2017).

[120] P. Krzysteczko, J. Wells, A. Fernández Scarioni, Z. Soban, T. Janda, X. Hu, V. Saidl, R.P. Campion, R. Mansell, J.-H. Lee, R.P. Cowburn, P. Nemec, O. Kazakova, J. Wunderlich, and H.W. Schumacher, Phys. Rev. B **95**, 220410 (2017).

[121] H. Corte-León, A.F. Scarioni, R. Mansell, P. Krzysteczko, D. Cox, D. McGrouther, S. McVitie, R. Cowburn, H.W. Schumacher, V. Antonov, and O. Kazakova, AIP Adv. **7**, 056808 (2017).

[122] E. Albisetti, D. Petti, M. Pancaldi, M. Madami, S. Tacchi, J. Curtis, W.P. King, A. Papp, G. Csaba, W. Porod, P. Vavassori, E. Riedo, and R. Bertacco, Nat. Nanotechnol. **11**, 1 (2016).

[123] Ó. Iglesias-Freire, M. Jaafar, E. Berganza, and A. Asenjo, Beilstein J. Nanotechnol. **7**, 1068 (2016).

[124] R. Nagatsu, M. Ohtake, M. Futamoto, F. Kirino, and N. Inaba, AIP Adv. **6**, 056503 (2016).

[125] M. Precner, J. Fedor, J. Tóbik, J. Šoltýs, and V. Cambel, Acta Phys. Pol. A **126**, 386 (2014).

[126] T. Wren, R. Puttock, B. Gribkov, S. Vdovichev, and O. Kazakova, Ultramicroscopy **179**, 41 (2017).

[127] T. Uhlig, U. Wiedwald, A. Seidenstücker, P. Ziemann, and L.M. Eng, Nanotechnology **25**, 255501 (2014).

[128] J.W. Alldredge and J. Moreland, J. Appl. Phys. **112**, 023905 (2012).

[129] J. Wells, A.F. Scarioni, H.W. Schumacher, D. Cox, R. Mansell, R. Cowburn, and O. Kazakova, AIP Adv. **7**, (2017).

[130] S. Vock, F. Wolny, T. Mühl, R. Kaltofen, L. Schultz, B. Büchner, C. Hassel, J. Lindner, and V. Neu, Appl. Phys. Lett. **97**, 252505 (2010).

[131] F. Wolny, T. Mühl, U. Weissker, A. Leonhardt, U. Wolff, D. Givord, and B. Büchner, J. Appl. Phys. **108**, 013908 (2010).

[132] Y. Lisunova, J. Heidler, I. Levkivskyi, I. Gaponenko, A. Weber, C. Caillier, L.J. Heyderman, M. Kläui, and P. Paruch, Nanotechnology **24**, 105705 (2013).

[133] H. Campanella, M. Jaafar, J. Llobet, J. Esteve, M. Vázquez, A. Asenjo, R.P. del Real, and J.A. Plaza, Nanotechnology **22**, 505301 (2011).

[134] J. Liu, W. Zhang, Y. Li, H. Zhu, R. Qiu, Z. Song, Z. Wang, and D. Li, J. Magn. Magn. Mater. **443**, 184 (2017).

[135] S. Ponomareva, L.F. Zanini, F. Dumas-Bouchiat, N.M. Dempsey, D. Givord, and F. Marchi, Adv. Mater. Res. **872**, 167 (2013).

[136] M. Rolandi, D. Okawa, S. a. Backer, A. Zettl, and J.M.J. Fréchet, J. Vac. Sci. Technol. B Microelectron. Nanom. Struct. **25**, L39 (2007).

[137] L.M. Belova, O. Hellwig, E. Dobisz, and E. Dan Dahlberg, Rev. Sci. Instrum. **83**, 093711 (2012).

[138] J.M. De Teresa, A. Fernández-Pacheco, R. Córdoba, L. Serrano-Ramón, S. Sangiao, and M.R. Ibarra, J. Phys. D. Appl. Phys. **49**, 243003 (2016).

[139] V. Neu, S. Vock, T. Sturm, and L. Schultz, Nanoscale **10**, 16881 (2018).

[140] S. McVitie, R.P. Ferrier, J. Scott, G.S. White, and A. Gallagher, J. Appl. Phys. **89**, 3656 (2001).

[141] M. Jaafar, A. Asenjo, and M. Vazquez, IEEE Trans. Nanotechnol. **7**, 245 (2008).

[142] P.J.A. van Schendel, H.J. Hug, B. Stiefel, S. Martin, and H.-J. Güntherodt, J. Appl. Phys. **88**, 435 (2000).

[143] V.N. Matveev, V.I. Levashov, V.T. Volkov, O. V Kononenko, A. V Chernyh, M.A. Knjazev, and V.A. Tulin, Nanotechnology **19**, 475502 (2008).

[144] A. Thiaville, L. Belliard, D. Majer, E. Zeldov, and J. Miltat, J. Appl. Phys. **82**, 3182 (1997).

[145] V. Panchal, O. Iglesias-Freire, A. Lartsev, R. Yakimova, A. Asenjo, and O. Kazakova, IEEE Trans. Magn. **49**, 3520 (2013).

[146] D. V. Ovchinnikov and a. a. Bukharaev, Tech. Phys. **46**, 1014 (2001).

[147] T. Häberle, F. Haering, H. Pfeifer, L. Han, B. Kuerbanjiang, U. Wiedwald, U. Herr, and B. Koslowski, New J. Phys. **14**, (2012).

[148] S. Sievers, K.-F. Braun, D. Eberbeck, S. Gustafsson, E. Olsson, H.W. Schumacher, and U. Siegner, Small **8**, 2675 (2012).

[149] A. Schillik, R. Shao, U. Herr, and B. Koslowski, IEEE Trans. Magn. **53**, 1 (2017).

[150] A. Körnig, M.A. Hartmann, C. Teichert, P. Fratzl, and D. Faivre, J. Phys. D. Appl. Phys. **47**, 235403 (2014).

[151] M. Serri, M. Mannini, L. Poggini, E. Vélez-Fort, B. Cortigiani, P. Sainctavit, D. Rovai, A. Caneschi, and R. Sessoli, Nano Lett. **17**, 1899 (2017).

[152] A. Benassi, M. a Marioni, D. Passerone, and H.J. Hug, Sci. Rep. **4**, 4508 (2014).

[153] N. Zingsem, F. Ahrend, S. Vock, D. Gottlob, I. Krug, H. Doganay, D. Holzinger, V. Neu, and A. Ehresmann, J. Phys. D. Appl. Phys. **50**, 495006 (2017).

[154] F. Rhein, T. Helbig, V. Neu, M. Krispin, and O. Gutfleisch, Acta Mater. **146**, 85 (2018).

[155] I. Lemesh, F. Büttner, and G.S.D. Beach, Phys. Rev. B **95**, 174423 (2017).

[156] F. Valdés-Bango, M. Vélez, L.M. Alvarez-Prado, J.M. Alameda, and J.I. Martín, AIP Adv. **7**, (2017).

[157] L. Tryputen, F. Guo, F. Liu, T.N.A. Nguyen, M.S. Mohseni, S. Chung, Y. Fang, J. Åkerman, R.D. McMichael, and C.A. Ross, Phys. Rev. B - Condens. Matter Mater. Phys. **91**, 1 (2015).

[158] A. Talapatra and J. Mohanty, J. Magn. Magn. Mater. **418**, 224 (2016).

[159] T.R. Albrecht, H. Arora, V. Ayanoor-Vitikkate, J.-M. Beaujour, D. Bedau, D. Berman, A.L. Bogdanov, Y.-A. Chapuis, J. Cushen, E.E. Dobisz, G. Doerk, He Gao, M. Grobis, B. Gurney, W. Hanson, O. Hellwig, T. Hirano, P.-O. Jubert, D. Kercher, J. Lille, Zuwei Liu, C.M. Mate, Y. Obukhov, K.C. Patel, K. Rubin, R. Ruiz, M. Schabes, Lei Wan, D. Weller, Tsai-Wei Wu, and En Yang, IEEE Trans. Magn. **51**, 1 (2015).

[160] X.K. Hu, S. Sievers, A. Müller, V. Janke, and H.W. Schumacher, Phys. Rev. B **84**, 024404 (2011).

[161] A. Kaidatzis, R.P. del Real, R. Alvaro, J. Luis Palma, J. Anguita, D. Niarchos, M. Vázquez, J. Escrig, and J.M. García-Martín, J. Phys. D. Appl. Phys. **49**, 175004 (2016).

[162] L.A. Rodríguez, C. Bran, D. Reyes, E. Berganza, M. Vázquez, C. Gatel, E. Snoeck, and A. Asenjo, ACS Nano **10**, 9669 (2016).

[163] M. Goiriena-Goikoetxea, K.Y. Guslienko, M. Rouco, I. Orue, E. Berganza, M. Jaafar, A. Asenjo, M.L. Fernández-Gubieda, L. Fernández Barquín, and A. García-Arribas, Nanoscale **9**, (2017).

[164] S. Ladak, D.E. Read, G.K. Perkins, L.F. Cohen, and W.R. Branford, Nat. Phys. **6**, 359 (2010).

[165] S. Díaz-Castañón, F. Leccabue, B.E. Watts, R. Yapp, A. Asenjo, and M. Vázquez, Mater. Lett. **47**, (2001).

[166] J. Park, B.L. Le, J. Sklenar, G.W. Chern, J.D. Watts, and P. Schiffer, Phys. Rev. B **96**, 1 (2017).

[167] M. Tanaka, E. Saitoh, H. Miyajima, T. Yamaoka, and Y. Iye, Phys. Rev. B **73**, 052411 (2006).

[168] S. Zhang, I. Gilbert, C. Nisoli, G.-W. Chern, M.J. Erickson, L. O'Brien, C. Leighton, P.E. Lammert, V.H.

Crespi, and P. Schiffer, Nature **500**, 553 (2013).

[169] S.A. Morley, S.T. Riley, J.-M. Porro, M.C. Rosamond, E.H. Linfield, J.E. Cunningham, S. Langridge, and C.H. Marrows, Sci. Rep. **8**, 4750 (2018).

[170] Y.-L. Wang, Z.-L. Xiao, A. Snezhko, J. Xu, L.E. Ocola, R. Divan, J.E. Pearson, G.W. Crabtree, and W.-K. Kwok, Science (80-.). **352**, 962 (2016).

[171] J.C. Gartside, D.M. Arroo, D.M. Burn, V.L. Bemmer, A. Moskalenko, L.F. Cohen, and W.R. Branford, Nat. Nanotechnol. 1 (2017).

[172] A. Dussaux, P. Schoenherr, K. Koumpouras, J. Chico, K. Chang, L. Lorenzelli, N. Kanazawa, Y. Tokura, M. Garst, A. Bergman, C.L. Degen, and D. Meier, Nat. Commun. **7**, 12430 (2016).

[173] G. Chen, Nat. Phys. **13**, 112 (2017).

[174] V.D. Nguyen, O. Fruchart, S. Pizzini, J. Vogel, J.C. Toussaint, and N. Rougemaille, Sci. Rep. **5**, 1 (2015).

[175] S.S.P. Parkin, M. Hayashi, and L. Thomas, Science (80-.). **320**, 190 (2008).

[176] G. Catalan, J. Seidel, R. Ramesh, and J.F. Scott, Rev. Mod. Phys. **84**, 119 (2012).

[177] A. Hubert and R. Schafer, *Magnetic Domains* (Springer Berlin Heidelberg, Berlin, Heidelberg, 1998).

[178] T. Shinjo, Science (80-.). **289**, 930 (2000).

[179] C. Moutafis, S. Komineas, C.A.F. Vaz, J.A.C. Bland, T. Shima, T. Seki, and K. Takanashi, Phys. Rev. B **76**, 104426 (2007).

[180] K. Yamada, S. Kasai, Y. Nakatani, K. Kobayashi, H. Kohno, A. Thiaville, and T. Ono, Nat. Mater. **6**, 270 (2007).

[181] R. Moriya, L. Thomas, M. Hayashi, Y.B. Bazaliy, C. Rettner, and S.S.P. Parkin, Nat. Phys. **4**, 368 (2008).

[182] M. Kammerer, M. Weigand, M. Curcic, M. Noske, M. Sproll, A. Vansteenkiste, B. Van Waeyenberge, H. Stoll, G. Woltersdorf, C.H. Back, and G. Schuetz, Nat. Commun. **2**, 279 (2011).

[183] C. Moreau-Luchaire, C. Moutafis, N. Reyren, J. Sampaio, C.A.F. Vaz, N. Van Horne, K. Bouzehouane, K. Garcia, C. Deranlot, P. Warnicke, P. Wohlhüter, J.M. George, M. Weigand, J. Raabe, V. Cros, and A. Fert, Nat. Nanotechnol. **11**, 444 (2016).

[184] C. Marrows, Physics (College. Park. Md). **8**, 40 (2015).

[185] S. Seki and M. Mochizuki, *Skyrmions in Magnetic Materials* (Springer International Publishing, Cham, 2016).

[186] T.H. O'Dell, Reports Prog. Phys. **49**, 589 (1986).

[187] J. McCord, J. Phys. D. Appl. Phys. **48**, (2015).

[188] S. Mittal, ACM J. Emerg. Technol. Comput. Syst. **13**, 1 (2016).

[189] J.C. Slonczewski, J. Magn. Magn. Mater. **159**, L1 (1996).

[190] L. Berger, Phys. Rev. B **54**, 9353 (1996).

[191] S. Parkin and S.-H. Yang, Nat. Nanotechnol. **10**, 195 (2015).

[192] I.M. Miron, G. Gaudin, S. Auffret, B. Rodmacq, A. Schuhl, S. Pizzini, J. Vogel, and P. Gambardella, Nat. Mater. **9**, 230 (2010).

[193] G. Bihlmayer, O. Rader, and R. Winkler, New J. Phys. **17**, 050202 (2015).

[194] J.E. Hirsch, Phys. Rev. Lett. **83**, 1834 (1999).

[195] S.-M. Seo, K.-W. Kim, J. Ryu, H.-W. Lee, and K.-J. Lee, Appl. Phys. Lett. **101**, 022405 (2012).

[196] M. Kläui, C.A.F. Vaz, J.A.C. Bland, L.J. Heyderman, F. Nolting, A. Pavlovska, E. Bauer, S. Cherifi, S. Heun, and A. Locatelli, Appl. Phys. Lett. **85**, 5637 (2004).

[197] V. Estévez and L. Laurson, Phys. Rev. B - Condens. Matter Mater. Phys. **91**, (2015).

[198] P. Bruno, Phys. Rev. Lett. **83**, 2425 (1999).

[199] D. Backes, C. Schieback, M. Kläui, F. Junginger, H. Ehrke, P. Nielaba, U. Rüdiger, L.J. Heyderman, C.S. Chen, T. Kasama, R.E. Dunin-Borkowski, C.A.F. Vaz, and J.A.C. Bland, Appl. Phys. Lett. **91**, 9 (2007).

[200] R. Allenspach and P.-O. Jubert, MRS Bull. **31**, 395 (2006).

[201] M. Lakshmanan, Philos. Trans. R. Soc. A Math. Phys. Eng. Sci. **369**, 1280 (2011).

[202] C. Bran, E. Berganza, E.M. Palmero, J.A. Fernandez-Roldan, R.P. Del Real, L. Aballe, M. Foerster, A. Asenjo, A. Fraile Rodríguez, and M. Vazquez, J. Mater. Chem. C **4**, 978 (2016).

[203] M. Yan, C. Andreas, A. Kákay, F. García-Sánchez, and R. Hertel, Appl. Phys. Lett. **99**, 122505 (2011).

[204] C.A. Ferguson, D.A. MacLaren, and S. McVitie, J. Magn. Magn. Mater. **381**, 457 (2015).

[205] Y.P. Ivanov, A. Chuvilin, L.G. Vivas, J. Kosel, O. Chubykalo-Fesenko, and M. Vázquez, Sci. Rep. **6**, 23844 (2016).

[206] P. Wohlhüter, M.T. Bryan, P. Warnicke, S. Gliga, S.E. Stevenson, G. Heldt, L. Saharan, A.K. Suszka, C. Moutafis, R.V. Chopdekar, J. Raabe, T. Thomson, G. Hrkac, and L.J. Heyderman, Nat. Commun. **6**, 7836 (2015).

[207] U.B. Arnalds, J. Chico, H. Stopfel, V. Kapaklis, O. Bärenbold, M.A. Verschuuren, U. Wolff, V. Neu, A. Bergman, and B. Hjörvarsson, New J. Phys. **18**, 023008 (2016).

[208] A. Koblischka-Veneva and M.R. Koblischka, J. Phys. Conf. Ser. **200**, 072053 (2010).

[209] K. Prashanthi, P.M. Shaibani, A. Sohrabi, T.S. Natarajan, and T. Thundat, Phys. Status Solidi - Rapid Res. Lett. **6**, 244 (2012).

[210] L.F. Henrichs, O. Cespedes, J. Bennett, J. Landers, S. Salamon, C. Heuser, T. Hansen, T. Helbig, O. Gutfleisch, D.C. Lupascu, H. Wende, W. Kleemann, and A.J. Bell, Adv. Funct. Mater. **26**, 2111 (2016).

[211] M. Estrader, A. López-Ortega, S. Estradé, I. V. Golosovsky, G. Salazar-Alvarez, M. Vasilakaki, K.N. Trohidou, M. Varela, D.C. Stanley, M. Sinko, M.J. Pechan, D.J. Keavney, F. Peiró, S. Suriñach, M.D. Baró, and J. Nogués, Nat. Commun. **4**, 1 (2013).

[212] M. Ghidini, R. Pellicelli, J.L. Prieto, X. Moya, J. Soussi, J. Briscoe, S. Dunn, and N.D. Mathur, Nat. Commun. **4**, 1421 (2013).

[213] N. Tran and T.J. Webster, J. Mater. Chem. **20**, 8760 (2010).

[214] J. Wells, O. Kazakova, O. Posth, U. Steinhoff, S. Petronis, L. Bogart, P. Southern, Q.A. Pankhurst, and C. Johansson, J. Phys. D. Appl. Phys. **21**, 428 (2017).

[215] R.M. Fratila, S. Rivera-Fernández, and J.M. de la Fuente, Nanoscale **7**, 8233 (2015).

[216] G. Cordova, B.Y. Lee, and Z. Leonenko, NanoWorld J **2**, 10 (2016).

[217] G. Datt, M. Sen Bishwas, M. Manivel Raja, and A.C. Abhyankar, Nanoscale **8**, 5200 (2016).

[218] C. Dong, S. Corsetti, D. Passeri, M. Rossi, M. Carafa, F. Pantanella, F. Rinaldi, C. Ingallina, A. Sorbo, and C. Marianecci, in *AIP Conf. Proc.* (2015), p. 020011.

[219] M. Jaafar, A.A.A. Aljabali, I. Berlanga, R. Mas-Ballesté, P. Saxena, S. Warren, G.P. Lomonossoff, D.J. Evans, and P.J. De Pablo, ACS Appl. Mater. Interfaces **6**, (2014).

[220] J. Pivetal, D. Royet, G. Ciuta, M. Frenea-Robin, N. Haddour, N.M. Dempsey, F. Dumas-Bouchiat, and P. Simonet, J. Magn. Magn. Mater. **380**, 72 (2015).

[221] W. Niu, K. Du, S. Wang, M. Zhang, M. Gao, Y. Chen, H. Liu, W. Zhou, F. Song, P. Wang, Y. Xu, X. Wang, J. Shen, and R. Zhang, Nanoscale **9**, 12372 (2017).

[222] T.M. Nocera, Y. Zeng, and G. Agarwal, Nanotechnology **25**, 461001 (2014).

[223] Q. Li, J. Song, M. Saura-Múzquiz, F. Besenbacher, M. Christensen, and M. Dong, Sci. Rep. **6**, 25985 (2016).

[224] X. Li, Z. Li, D. Pan, S. Yoshimura, and H. Saito, Appl. Phys. Lett. **104**, 213106 (2014).

[225] X. Li, W. Lu, Y. Song, Y. Wang, A. Chen, B. Yan, S. Yoshimura, and H. Saito, Sci. Rep. **6**, 22467 (2016).

[226] D. Kim, N.K. Chung, S. Allen, S.J.B. Tendler, and J.W. Park, ACS Nano **6**, 241 (2012).

[227] D. Passeri, C. Dong, M. Reggente, L. Angeloni, M. Barteri, F.A. Scaramuzzo, F. De Angelis, F. Marinelli, F. Antonelli, F. Rinaldi, C. Marianecci, M. Carafa, A. Sorbo, D. Sordi, I.W. Arends, and M. Rossi, Biomatter **4**, e29507 (2014).

[228] A.M. Gilbertson, H. Sadeghi, V. Panchal, O. Kazakova, C.J. Lambert, S.A. Solin, and L.F. Cohen, Appl. Phys. Lett. **107**, (2015).

[229] E. Zueco, W. Rave, R. Schäfer, M. Mertig, and L. Schultz, J. Magn. Magn. Mater. **196**–**197**, 115 (1999).

[230] E. Zueco, W. Rave, R. Schäfer, A. Hubert, and L. Schultz, J. Magn. Magn. Mater. **190**, 42 (1998).

[231] U. Mick, V. Eichhorn, T. Wortmann, C. Diederichs, and S. Fatikow, in *2010 IEEE Int. Conf. Robot. Autom.* (IEEE, 2010), pp. 4088–4093.

[232] C. Shi, D.K. Luu, Q. Yang, J. Liu, J. Chen, C. Ru, S. Xie, J. Luo, J. Ge, and Y. Sun, Microsystems Nanoeng. **2**, 16024 (2016).

[233] C. Yang, R. Winkler, M. Dukic, J. Zhao, H. Plank, and G.E. Fantner, ACS Appl. Mater. Interfaces **9**, 24456 (2017).

[234] T. Ando, Nanotechnology **23**, 062001 (2012).

[235] A.N. Moores and A.J. Cadby, Rev. Sci. Instrum. **89**, 023708 (2018).

[236] A. V Moskalenko, P.L. Yarova, S.N. Gordeev, and S. V Smirnov, Biophys. J. **98**, 478 (2010).

[237] J.C. Gartside, D.M. Burn, L.F. Cohen, and W.R. Branford, Sci. Rep. **6**, 32864 (2016).

[238] L. Hirt, S. Ihle, Z. Pan, L. Dorwling-Carter, A. Reiser, J.M. Wheeler, R. Spolenak, J. Vörös, and T. Zambelli, Adv. Mater. **28**, 2311 (2016).

[239] J.M. Englert, P. Vecera, K.C. Knirsch, R.A. Schäfer, F. Hauke, and A. Hirsch, ACS Nano **7**, 5472 (2013).

[240] F. Tang, P. Bao, A. Roy, Y. Wang, and Z. Su, Polym. (United Kingdom) **142**, 155 (2018).

[241] Y.F. Dufrêne, T. Ando, R. Garcia, D. Alsteens, D. Martinez-Martin, A. Engel, C. Gerber, and D.J. Müller, Nat. Nanotechnol. **12**, 295 (2017).

[242] S. Wegmann, I.D. Medalsy, E. Mandelkow, and D.J. Müller, Proc. Natl. Acad. Sci. **110**, E313 (2013).

[243] S. V. Kalinin, E. Strelcov, A. Belianinov, S. Somnath, R.K. Vasudevan, E.J. Lingerfelt, R.K. Archibald, C. Chen, R. Proksch, N. Laanait, and S. Jesse, ACS Nano **10**, 9068 (2016).

[244] L. Collins, A. Belianinov, R. Proksch, T. Zuo, Y. Zhang, P.K. Liaw, S. V. Kalinin, and S. Jesse, Appl. Phys. Lett. **108**, 193103 (2016).

[245] D. Nečas and P. Klapetek, Cent. Eur. J. Phys. **10**, 181 (2012).

[246] J. Ahrens, B. Geveci, and C. Law, *ParaView: An End-User Tool for Large Data Visualization* (Elsevier, 2005).

[247] U. Ayachit, *The ParaView Guide: A Parallel Visualization Application* (Kitware, 2015).

[248]Http://Www.Smarttip.Nl/Products/Spm-Probes/Magnetic-Probes (n.d.).

[249] W. Dickson, S. Takahashi, R. Pollard, R. Atkinson, and A.V. Zayats, IEEE Trans. Nanotechnol. **4**, 229 (2005).

[250] P. Dorozhkin, E. Kuznetsov, A. Schokin, S. Timofeev, and V. Bykov, Micros. Today **18**, 28 (2010).

[251] D. Holzinger, I. Koch, S. Burgard, and A. Ehresmann, ACS Nano **9**, 7323 (2015).

[252] S.D. Granz and M.H. Kryder, J. Magn. Magn. Mater. **324**, 287 (2012).

[253] S. Okamoto, N. Kikuchi, M. Furuta, O. Kitakami, and T. Shimatsu, J. Phys. D. Appl. Phys. **48**, (2015).

[254] Y.J. Chen, H.Z. Yang, S.H. Leong, K.M. Cher, J.F. Hu, P. Sethi, and W.S. Lew, J. Appl. Phys. **117**, 17D117 (2015).

[255] Y.J. Chen, H.Z. Yang, S.H. Leong, B. Santoso, J.Z. Shi, B.X. Xu, and J.W.H. Tsai, J. Appl. Phys. **117**, 17C106 (2015).

[256] C. Marrows, Science (80-.). **351**, 558 (2016).

[257] T. Jungwirth, X. Marti, P. Wadley, and J. Wunderlich, Nat. Nanotechnol. **11**, 231 (2016).

[258] P. Wadley, V. Novák, R.P. Campion, C. Rinaldi, X. Martí, H. Reichlová, J. Železný, J. Gazquez, M.A. Roldan, M. Varela, D. Khalyavin, S. Langridge, D. Kriegner, F. Máca, J. Mašek, R. Bertacco, V. Holý, A.W. Rushforth, K.W. Edmonds, B.L. Gallagher, C.T. Foxon, J. Wunderlich, and T. Jungwirth, Nat. Commun. **4**, 2322 (2013).

[259] D. Halley, N. Najjari, H. Majjad, L. Joly, P. Ohresser, F. Scheurer, C. Ulhaq-Bouillet, S. Berciaud, B. Doudin, and Y. Henry, Nat. Commun. **5**, 3167 (2014).

[260] P. Borisov, A. Hochstrat, V. V. Shvartsman, W. Kleemann, and P.M. Hauck, Integr. Ferroelectr. **99**, 69 (2008).

[261] D. Khomskii, Physics (College. Park. Md). **2**, 20 (2009).

[262] I. Sugiyama, N. Shibata, Z. Wang, S. Kobayashi, T. Yamamoto, and Y. Ikuhara, Nat. Nanotechnol. **8**, 266 (2013).

[263] G.E.W. Bauer, E. Saitoh, and B.J. van Wees, Nat. Mater. **11**, 391 (2012).

[264] J.P. Heremans, Nature **508**, 327 (2014).

[265] F. J. Di Salvo, Science (80-.). **285**, 703 (1999).

[266] A. Sola, P. Bougiatioti, M. Kuepferling, D. Meier, G. Reiss, M. Pasquale, T. Kuschel, and V. Basso, Sci. Rep. **7**, 1 (2017).

[267] K. Uchida, J. Xiao, H. Adachi, J. Ohe, S. Takahashi, J. Ieda, T. Ota, Y. Kajiwara, H. Umezawa, H. Kawai, G.E.W. Bauer, S. Maekawa, and E. Saitoh, Nat. Mater. **9**, 894 (2010).

[268] C. Hahn, G. de Loubens, M. Viret, O. Klein, V. V. Naletov, and J. Ben Youssef, Phys. Rev. Lett. **111**, 217204 (2013).

[269] V. Castel, N. Vlietstra, B.J. Van Wees, and J. Ben Youssef, Phys. Rev. B - Condens. Matter Mater. Phys. **86**, 1 (2012).

[270] K. Harii, T. An, Y. Kajiwara, K. Ando, H. Nakayama, T. Yoshino, and E. Saitoh, J. Appl. Phys. **109**, 116105 (2011).

[271] Y. Kajiwara, K. Harii, S. Takahashi, J. Ohe, K. Uchida, M. Mizuguchi, H. Umezawa, H. Kawai, K. Ando, K. Takanashi, S. Maekawa, and E. Saitoh, Nature **464**, 262 (2010).

[272] M.I. Dyakonov and V.I. Perel, Phys. Lett. A **35**, 459 (1971).

[273] S. Zhang, Phys. Rev. Lett. **85**, 393 (2000).

[274] T. Kimura, Y. Otani, T. Sato, S. Takahashi, and S. Maekawa, Phys. Rev. Lett. **98**, 156601 (2007).

[275] Y. Niimi and Y. Otani, Reports Prog. Phys. **78**, 124501 (2015).

[276] J. Sinova, S.O. Valenzuela, J. Wunderlich, C.H. Back, and T. Jungwirth, Rev. Mod. Phys. **87**, 1213 (2015).

[277] K. Uchida, S. Takahashi, K. Harii, J. Ieda, W. Koshibae, K. Ando, S. Maekawa, and E. Saitoh, Nature **455**, 778 (2008).

[278] C.M. Jaworski, J. Yang, S. Mack, D.D. Awschalom, J.P. Heremans, and R.C. Myers, Nat. Mater. **9**, 898 (2010).

[279] S.Y. Huang, X. Fan, D. Qu, Y.P. Chen, W.G. Wang, J. Wu, T.Y. Chen, J.Q. Xiao, and C.L. Chien, Phys. Rev. Lett. **109**, 107204 (2012).

[280] Y. Shiomi, T. Ohtani, S. Iguchi, T. Sasaki, Z. Qiu, H. Nakayama, K. Uchida, and E. Saitoh, Appl. Phys. Lett. **104**, 0 (2014).

[281] S.M. Wu, J. Hoffman, J.E. Pearson, and A. Bhattacharya, Appl. Phys. Lett. **105**, 092409 (2014).

[282] X. Liang, Y. Zhu, B. Peng, L. Deng, J. Xie, H. Lu, M. Wu, and L. Bi, ACS Appl. Mater. Interfaces **8**, 8175 (2016).

[283] S. Geprägs, S.T.B. Goennenwein, M. Schneider, F. Wilhelm, K. Ollefs, A. Rogalev, M. Opel, and R. Gross, ArXiv1307.4869v1 [Cond-Mat.Mtrl-Sci] 18 Jul 2013 **110**, 5 (2013).

[284] J.F.K. Cooper, C.J. Kinane, S. Langridge, M. Ali, B.J. Hickey, T. Niizeki, K. Uchida, E. Saitoh, H. Ambaye, and A. Glavic, Phys. Rev. B **96**, 1 (2017).

[285] M. Weiler, M. Althammer, F.D. Czeschka, H. Huebl, M.S. Wagner, M. Opel, I.M. Imort, G. Reiss, A. Thomas, R. Gross, and S.T.B. Goennenwein, Phys. Rev. Lett. **108**, 1 (2012).

[286] A. Fert, V. Cros, and J. Sampaio, Nat. Nanotechnol. **8**, 152 (2013).

[287] A.K. Nayak, V. Kumar, T. Ma, P. Werner, E. Pippel, R. Sahoo, F. Damay, U.K. Rößler, C. Felser, and S.S.P. Parkin, Nature **548**, 561 (2017).

[288] K. Litzius, I. Lemesh, B. Krüger, P. Bassirian, L. Caretta, K. Richter, F. Büttner, K. Sato, O.A. Tretiakov, J.

Förster, R.M. Reeve, M. Weigand, I. Bykova, H. Stoll, G. Schütz, G.S.D. Beach, and M. Kläui, Nat. Phys. **13**, 170 (2016).

[289] A. Neubauer, C. Pfleiderer, B. Binz, A. Rosch, R. Ritz, P.G. Niklowitz, and P. Böni, Phys. Rev. Lett. **102**, 186602 (2009).

[290] K. Hamamoto, M. Ezawa, and N. Nagaosa, Appl. Phys. Lett. **108**, 1 (2016).

[291] D. Andrikopoulos and B. Sorée, Sci. Rep. **7**, 1 (2017).

[292] K. Tanabe and K. Yamada, Appl. Phys. Lett. **110**, (2017).

[293] S. Mühlbauer, Science (80-.). **333**, 1381 (2011).

[294] X.Z. Yu, Y. Onose, N. Kanazawa, J.H. Park, J.H. Han, Y. Matsui, N. Nagaosa, and Y. Tokura, Nature **465**, 901 (2010).

[295] S.L. Zhang, A. Bauer, D.M. Burn, P. Milde, E. Neuber, L.M. Eng, H. Berger, C. Pfleiderer, G. Van Der Laan, and T. Hesjedal, Nano Lett. **16**, 3285 (2016).

[296] W. Jiang, G. Chen, K. Liu, J. Zang, S.G.E. te Velthuis, and A. Hoffmann, Phys. Rep. **704**, 1 (2017).

[297] W. Legrand, D. Maccariello, N. Reyren, K. Garcia, C. Moutafis, C. Moreau-Luchaire, S. Collin, K. Bouzehouane, V. Cros, and A. Fert, Nano Lett. **17**, 2703 (2017).

[298] N. Nagaosa and Y. Tokura, Nat. Nanotechnol. **8**, 899 (2013).

[299] F. Büttner, I. Lemesh, M. Schneider, B. Pfau, C.M. Günther, P. Hessing, J. Geilhufe, L. Caretta, D. Engel, B. Krüger, J. Viefhaus, S. Eisebitt, and G.S.D. Beach, Nat. Nanotechnol. **12**, 1040 (2017).

[300] S. Woo, K. Litzius, B. Krüger, M.Y. Im, L. Caretta, K. Richter, M. Mann, A. Krone, R.M. Reeve, M. Weigand, P. Agrawal, I. Lemesh, M.A. Mawass, P. Fischer, M. Kläui, and G.S.D. Beach, Nat. Mater. **15**, 501 (2016).

[301] W. Jiang, P. Upadhyaya, W. Zhang, G. Yu, M.B. Jungfleisch, F.Y. Fradin, J.E. Pearson, Y. Tserkovnyak, K.L. Wang, O. Heinonen, S.G.E. Te Velthuis, and A. Hoffmann, Science (80-.). **349**, 283 (2015).

[302] M. Baćani, M.A. Marioni, J. Schwenk, and H.J. Hug, ArXiv 1 (2016).

[303] S. Zhang, J. Zhang, Q. Zhang, C. Barton, V. Neu, Y. Zhao, Z. Hou, Y. Wen, C. Gong, O. Kazakova, W. Wang, Y. Peng, D.A. Garanin, E.M. Chudnovsky, and X. Zhang, Appl. Phys. Lett. **112**, 132405 (2018).

[304] W. Wang, F. Yang, C. Gao, J. Jia, G.D. Gu, and W. Wu, APL Mater. **3**, 083301 (2015).

[305] J. Yi, H. Zhuang, Q. Zou, Z. Wu, G. Cao, S. Tang, S.A. Calder, P.R.C. Kent, D. Mandrus, and Z. Gai, 2D Mater. **4**, 011005 (2016).

[306] F. Moro, M.A. Bhuiyan, Z.R. Kudrynskyi, R. Puttock, O. Kazakova, O. Makarovsky, M.W. Fay, C. Parmenter, Z.D. Kovalyuk, A.J. Fielding, M. Kern, J. van Slageren, and A. Patanè, Adv. Sci. **1800257**, 1800257 (2018).

[307] H. Li, X. Qi, J. Wu, Z. Zeng, J. Wei, and H. Zhang, ACS Nano **7**, 2842 (2013).

[308] L.H. Li and Y. Chen, J. Appl. Phys. **116**, 213904 (2014).

[309] S. Yang, C. Wang, H. Sahin, H. Chen, Y. Li, S.-S. Li, A. Suslu, F.M. Peeters, Q. Liu, J. Li, and S. Tongay, Nano Lett. **15**, 1660 (2015).

[310] T. Ando, T. Uchihashi, and N. Kodera, Annu. Rev. Biophys. **42**, 393 (2013).

[311] A. Ortega-Esteban, K. Bodensiek, C. San Martín, M. Suomalainen, U.F. Greber, P.J. de Pablo, and I.A.T.

Schaap, ACS Nano **9**, 10571 (2015).

[312] I. Slabu, G. Guntherodt, T. Schmitz-Rode, M. Hodenius, N. Kramer, H. Donker, G. A. Krombach, J. Otto, U. Klinge, and M. Baumann, Curr. Pharm. Biotechnol. **13**, 545 (2012).

[313] Q. Liu, A.P. Roberts, J.C. Larrasoaña, S.K. Banerjee, Y. Guyodo, L. Tauxe, and F. Oldfield, Rev. Geophys. **50**, RG4002 (2012).

[314] P. Liu and Y. Hong, in *Magn. Nanomater. - Fundam. Synth. Appl.* (Wiley-VCH Verlag GmbH & Co. KGaA, Weinheim, Germany, 2017), pp. 515–546.

[315] S. Mirshahghassemi and J.R. Lead, Environ. Sci. Technol. **49**, 11729 (2015).

[316] R. Nisticò, Res. Chem. Intermed. **43**, 6911 (2017).